DEUTSCHES ELEKTRONEN-SYNCHROTRON DESY

DESY 66/27
Oktober 1966
Experimente

Elastic Electron-Proton Scattering at Momentum Transfers up to 110 Fermi^{-2}

by

H. J. Behrend, F. W. Brasse, J. Engler and H. Hultschig
Deutsches Elektronen-Synchrotron DESY, Hamburg

S. Galster, G. Hartwig and H. Schopper
Institut für Experimentelle Kernphysik der Technischen Hochschule
und des Kernforschungszentrums Karlsruhe

E. Ganssauge
Physikalisches Intitut der Universität Marburg

2 HAMBURG 52 · NOTKESTIEG 1

ELASTIC ELECTRON-PROTON SCATTERING AT MOMENTUM TRANSFERS UP TO 110 FERMI^{-2}

Submitted to IL NUOVO CIMENTO

H.J. Behrend, F.W. Brasse, J. Engler and H. Hultschig
Deutsches Elektronen Synchrotron - Hamburg

S. Galster, G. Hartwig and H. Schopper
Institut für Experimentelle Kernphysik der Technischen Hochschule und des Kernforschungszentrums Karlsruhe - Karlsruhe

E. Ganssauge
Physikalisches Institut der Universität - Marburg

Summary.- Using the internal beam of DESY elastic electron-proton cross sections were measured at various angles between 32^{o} and 130^{o}, and with momentum transfers of q^2= 39, 6o, 8o, and 110 f^{-2}. Two single quadrupole spectrometers, movable around a common liquid-hydrogen target, were used for analysing the momentum of the scattered electrons. Čerenkov and shower counters discriminated against pion and low-energy background. As a cross section reference recoil protons from elastic scattering at q^2=10 f^{-2} were used, with a quantameter serving as an intermediate monitor. The data are consistent with the Rosenbluth formula, giving real form factors G_E and G_M. Both continue to decrease with increasing momentum transfer, but somewhat faster than indicated by previous measurements.

1.- Introduction.

Electron scattering experiments for investigating the structure of the proton have been done at Cornell, Cambridge, Orsay, and most intensively at Stanford. The data obtained showed that the proton has an extended structure which causes the cross section to drop rapidly below the value corresponding to a point proton.

Theoretical discussions lead to the conclusion that the proton can be described by introducing two independent amplitudes commonly called form factors in analogy to the non-relativistic scattering. Usually the so-called electric and magnetic form factors G_E and G_M are chosen, which in the static limit are the electric charge e and the magnetic moment μ of the proton and whose gradients at $q^2=0$ are proportional to the mean square radius of the corresponding distributions [1]-[3].

The cross section calculated in the first Born approximation (one-photon exchange) is given by the well known Rosenbluth formula [4], by means of which the form factors are calculated from the measured cross sections. Untill now, the Rosenbluth formula has been proved to hold up to a momentum transfer of $q^2=45\ f^{-2}$ and for scattering angles larger than 30^o [3].

In this experiment cross sections were measured for testing the Rosenbluth straight line at $q^2= 39$, 60, and 80 f^{-2}. The measurements were done by deflecting the internal beam of the DESY onto a liquid-hydrogen target, which was placed in the vacuum chamber of the synchrotron. Since an absolute monitoring device - such as a Faraday cup - could not be used, we chosed for reference the elastic cross section at $q^2=10\ f^{-2}$. This is different from the bremsstrahlung reference usually chosen. When the total bremsstrahlung cross section is used as a reference the following three main errors are introduced into the cross section: 1) the uncertainty of the quantameter constant of about 3% with a possibly existing time dependence of the constant, 2)

the uncertainty of at least 3% in determining the bremsstrahlung coming from the target wall, and 3) the uncertainty of the calculated radiation length, which is estimated to be 3% [5]. This amounts to an over-all error of at least 6%. Therefore we used the quantameter reading only as an intermediate normal and measured at each setting of any incident energy the recoiling protons at $q^2=10\ f^{-2}$. From measurements with a Faraday cup as a monitor [6],[7], the form factors in this region are well known such that the errors in the corresponding cross sections are only 3%, assuming the Rosenbluth formula to remain valid.

To ensure that there occurs at least no gross deviation from the Rosenbluth straight line at $q^2=10\ f^{-2}$ for high primary energy E_o, we measured the cross sections at E_o = 3.5, 4.0 and 6.0 GeV based on the bremsstrahlung, the correction for which could be estimated more accurately in this high energy region than at low energies.

In Sect. 2 the experimental arrangement is described. In Sect. 3 the technique of data taking and the method of analysing the data are explained including a discussion of the estimated errors. The cross sections and the extracted form factors are given in Sect. 4, and the conclusions of the present work are given in Sect. 5.

2.- The Experimental Arrangement.

A survey of the apparatus is shown in Fig.1. Two nearly identical spectrometers, each consisting of one quadrupole, could be moved around a common pivot located underneath the target. The angles accessible to the spectrometers were 54°-135° and 32°-90° for spectrometer 1 and spectrometer 2 respectively.

2.1.-The internal beam striking the target.

At the end of the accelerating period of the synchrotron the beam was shifted towards the target by turning off the radio-frequency voltage before the field in the synchrotron magnets reached its

maximum value B_{max}. The spill time, during which the beam hits the target, was limited to ±300μsec relative to B_{max}, resulting in an energy spread of 0.0%-0.3%. The effective spill time was much shorter, typically 40 μsec at low energies and 100-200 μsec at energies greater than 3 GeV.

The momentum resolution of a one-quadrupole spectrometer depends mainly on the vertical beam spread on the target. Therefore we limited the zone where the beam hit the target by two movable tungsten scrapers located 2.06 betatron wave lengths upstream from the target. With the two scrapers a slit was formed of usually 4-6 mm in the vertical direction. This was a compromise between a good momentum resolution in the spectrometers and not too low an intensity on the target. With the slit width chosen the effective intensity at the target was reduced by a factor of two.

In addition we used a horizontally movable scraper block, whose image was typically positioned 10 mm behind the front of the target to ensure that nothing else but the target was struck by the beam.

Determination of the energy.- The energy of the primary electrons must be determined with accuracy, because an uncertainty in the primary energy of 1% results in an uncertainty of around 4% in the cross section.

The synchrotron energy scale was calibrated with a pair spectrometer by measuring the curvature of electron and positron pairs produced by bremsstrahlung (8). In order to obtain the energy of the electrons hitting the target, corrections for target position, spill time etc. have to be taken into account.

In addition to the pair-spectrometer calibration, the primary energy E_o below 2 GeV could be determined by observing electron-proton coincidences. From the angles of the two spectrometers one obtains

$$E_o = M\,(\mathrm{cotg}\phi \cdot \mathrm{cotg}\theta/2 - 1),$$

where θ is the angle of the scattered electron,
and ϕ is the angle of the recoiling proton.
Such determinations we made several times. Knowing E_o the calibration constants for the two quadrupole spectrometers could be determined from the kinematics of the elastic scattering. They were in agreement with those obtained from measurements with α-particles and floating wire.
For each measurement the primary energy was determined from the energy E' of the scattered electron and θ via the elastic kinematics

$$E_o = \frac{E'}{1 - \frac{2E'}{M}\sin^2\theta/2}\,.$$

The accuracy of the energy determination was estimated to be 0.3%.

2.2.- The liquid-hydrogen target.

The target was similar to that used by the Harvard group[9]. By means of liquid helium about 10 liters of hydrogen gas out of a 20 liter reservoir were liquified and dropped into a target cup. When using a transfer system for the helium which was constructed at DESY, only 2.7 liter/h of liquid helium were needed. The cup cylinder was 11 mm in diameter and 40 mm high, the wall being made of 12 μ thick Polyimid foil from DuPont. This foil is very resistant against radiation: no foil was broken, the longest exposure to the beam having been 100 h at a circulating current of 3 mA. From photographs of the boiling hydrogen we estimated the density reduction due to the bubbles at 5%. This effect did not enter into the cross section calculations; only for the q^2=10 f^{-2} points obtained by way of the bremsstrahlung calibration this effect resulted in a correction on the order of 0.5%.
For the usual scraper slit of 4-6mm we estimated the number of multiple traversals through the target from the measured current in the machine and the collected charge in the quantameter to be 2 at 2 GeV and 3 at 4 GeV.

The target could be moved vertically and horizontally within a range of 40 mm. The closest approach to the equilibrium orbit was 10 mm, and a typical distance used was 15 mm.

2.3.-The quantameter.

The quantameter monitored the total energy of the bremsstrahlung, which is proportional to the product of the incident electron flux and the total thickness traversed, thus relating the cross section to the radiation length of the target material.
The quantameter used was of the Wilson type [10], with the shower-absorbing sandwich consisting of polished copper plates and a gas mixture of 95% Ar and 5% CO_2. The collected charge was integrated by a integrator device, designed and built at DESY by H. Pingel.
It works as follows: The incoming charge has to neutralise a capacitors charge, which is independent from the absolute value of the capacitor, since it had been loaded by a definite current during the closing time of a relay. The time is measured to an accuracy of 10^{-4}. The integrator has a long-time stability of 0.3%. The whole uncertainty in the charge integration (calibration, dark current in the amplifier etc.) was estimated to be 0.5%.
The quantameter was calibrated with the external beam of DESY against a Faraday cup and a calorimeter. The measured quantameter constant κ, which relates the number of effective quanta N_{eff} to the measured amount of charge Q, $N_{eff}=\kappa \cdot Q/E_o$, was found to be

$$\kappa = 4.53 \cdot 10^{+18} \text{ MeV/Coulomb.}$$

This constant turned out to be quite dependent on the intensity of the γ-beam. The above value corresponds to an intensity of 10^6 effective quanta in a time interval of 50 μsec, which was the typical intensity when the measurements of therecoil protons at $q^2=10\ f^{-2}$ for testing the Rosenbluth formula were made.
The distance from the quantameter to the target was 10 m. The quantameter was shielded against background by a concrete bunker, and the open window corresponded to a half angle of 1.0^o.
The influence of the vacuum chamber (projected thickness 15 mm Al) on

the quantameter reading was calculated amounting to a loss of 3% at 4 GeV. By putting additional plates in the beam and extrapolating to zero wall thickness this result was confirmed.

2.4.- The spectrometer set-up.

Spectrometer 1 consisted of a halved quadrupole (DESY type QC) with a relatively large aperture but short magnetic length. It was designed for measurements at large angles up to 135°. The quadrupole of spectrometer 2 (DESY type QA) has a longer magnetic length (1.0 m) but a smaller aperture than QC, it could analyse a maximum momentum of 3 GeV/c.

Fig. 2 shows a cut of a spectrometer arrangement. The scattered particles were focused vertically by a quadrupole onto the momentum defining scintillation counters, yielding a dispersion of 4.43 cm per $\Delta p/p = 1\%$ (spectrometer 2). A central lead plug in the magnet shadowed the counters from the direct view of the target and absorbed weakly bended particles which would otherwise deteriorate the momentum resolution. Because of the large background, a pure momentum analysis was not sufficient for identifying the elastic events. Electrons were therefore discriminated against pions and other particles by a threshold Čerenkov counter and a subsequent shower counter. Protons were identified by their high ionisation loss dE/dx in a scintillation counter.

The scattering angle.- The scattering angle is defined as the angle subtended by the central line of the bremsstrahlung beam emerging from the target and the geometrical center of the spectrometer. This angle could be read to 0.05° from a fiducial circle with its center on the pivot. The zero mark of the circle was measured relative to the direction of the bremsstrahlung before our measurements and a second time in between. The resulting difference of 0.03° was within the precision of the measurement.

The angle read from the fiducial circle had to be corrected for the target not situated exactly above the pivot. Two further corrections arise from the finite aperture of the quadrupoles: 1) The decrease of the cross section with increasing angles causes the center of the aperture to be shifted towards smaller angles. This shifting depends on the energy and the angle and varied from 0.05 to 0.20°. 2) The azimuthal center of the

aperture had to be projected onto the horizontal scattering plane along the line where the cone of the scattered particles cuts the plane of the spectrometer. This shift was 0.10° at 32° and zero at 90°. The uncertainty in the corrected angles was estimated to be 0.05°.

The solid angle. - In front of the quadrupoles there were 10 cm thick lead collimators so that no particles coming from the target could hit the vacuum chamber inside the magnet. These lead collimators and the central stoppers defined the solid angles. At spectrometer 2 lead blocks could be moved in front of the fixed collimator in order to change the horizontal and vertical opening of the spectrometer. The collimator system of spectrometer 2 was positioned at 40 cm from the magnetic end of the quadrupole. Thus the solid angle was defined by the geometrical opening. The limiting trajectories for the collimator of spectrometer 2 and the two stoppers had been calculated with an analog computer. The solid angles were

$$\Delta\Omega_{\text{spectr. 1}} = (6.9 \pm 0.05) \text{ msterad}$$

$$\Delta\Omega_{\text{spectr. 2}} = (3.55 \pm 0.02) \text{ msterad}$$

In measuring recoil protons with spectrometer 2, the horizontal aperture had to be narrowed because of the strong dependence of the proton momentum on the scattering angle. The solig angle was

$$d\Omega_{\text{proton}} = (1.65 \pm 0.02) \text{ msterad.}$$

The momentum defining counters. - The momentum was determined with the slat counters labelled 2,3,4,5 in Fig. 2, their separation corresponded to a momentum difference of 1.5%. The effective width of one counter due to the finite hight was 1.35%.

The cross section was measured with the split counters 11,12, 61, 62 by the flat top method. In a crossed coincidence (11, 62 and 12, 61) they worked like a broad infinitesimal flat counter. The distance of the two pairs corresponded to $\Delta p/p = 6.85\%$. This was nearly three times the momentum resolution, so that the flat-top method was quite acceptable. At spectrometer 1 the distance corresponded to about $\Delta p/p = 4.5\%$, which was just sufficient for giving a flat top.

In the horizontal direction the long scintillators (type NE102) were split in two parts in order to fit the image line as determined by floating wire and α-ray measurements. Each part was separately viewed by a 56 AVP photomultiplier.

The counters were mounted on banks which could be rotated aground a vertical axis to compensate for the variation of particle momentum with the scattering angle across the spectrometer aperture. The banks were also movable in the vertical direction and could thus be adjusted with respect to the center of the target image. The counter bank was in the right position when the two momentum foci appeared at the same quadrupole current for particles coming out of the upper and lower halves of the quadrupole.

The small angles of the trajectories respective to the horizontal plane necessitated careful alignment of the counter bank. The scintillator edges were aligned to ± 0.2 mm with respect to the medium horizontal plane.

The particle defining counters. - The two identical Čerenkov counters, each 0.8 m long, were filled with Frigen 13 (CF_3Cl). The optical system consisted of five spherical mirrors which concentrated the Čerenkov radiation on five 56 UVP tubes in optical contact with quartz glass windows in the tank. The mirrors were produced by pressing hot plexiglass and covering it with a thin aluminium layer, which was coated for protection with quartz.

The efficiency of the Čerenkov counters was determined at a point of low momentum transfer by comparing the yield of elastic electrons with and without the Čerenkov counter in coincidence. The efficiency could also be estimated by extrapolating the pulse height spectrum below the discrimination level (Fig. 3). Both methods yielded (99.3 ± 0.2)% efficiency at 7 atmospheres.

The two shower counters were not identical. At spectrometer 2 a sandwich was used, consisting of 4 lead plates of one radiation length each, and 4 scintillators all in optical contact with one photomultiplier. A pulse height spectrum is shown in Fig. 4. By extrapolating the electron spectrum below the discriminator level the efficiency was calculated, typically being 90% - 98%. Spectrometer 2 used 3 radiation

lengths of Pb followed by a scintillator plate. The correlation between shower and Čerenkov pulses enabled us to obtain better analysis through application of a two-dimensional pulse-height analyser (Fig.5).
In spectrometer 2 an additional scintillator plate between the counter bank and the Čerenkov counter served as a dE/dx counter for proton measurements. It was viewed by two photomultipliers with equal light transfer to both sides, giving an uniform light output over the whole area.

2.5.- The electronic logic.

A 100 Mc commercial electronics system was used. The pulses transferred by 150 m of 3/8" cables to the counting station were clipped before entering the discriminators. The output pulses from the discriminators were clipped similarly, which lead to a resolving time of 8 nsec for the coincidences.
First of all, the coincidences $\overline{11,62}$ and $\overline{12,61}$ were established, giving the broad momentum definition, which was followed by the Čerenkov counter and the shower counter coincidences. The final coincidences were those with the slat counters. The coincidences involving the shower counter were doubled because analysis was made for two different discriminator levels.
Random coincidences were indicated by delayed coincidences at various stages in the logic. In order to obtain a reliable information of the actual random coincidences in the four-fold coincidence, a four-fold coincidence unit was used, the output of which had a length proportional to the overlapping time of the incomming pulses. The stretched pulses were observed on an x-y storage oscilloscope in correlation with the Čerenkov pulses. No more than about five per cent random coincidences were allowed.

3.- Data Taking and Analysis.

3.1.- Magnet setting.

A momentum spectrum of the scattered electrons taken at a high counting rate (low momentum transfer) is shown in Fig.6, in which the rate of the crossed coincidence (OR) and the coincidence rate with the slat counters are plotted. The elastic yield can easily be taken to be the difference between the flat top and the extrapolated background in the OR-rate. The relative amount of background beneath the flat top can also be calculated by the shape of the elastic peak obtained with the slat counters. For the latter case only a few points of the momentum spectrum had to be taken.
Therefore the magnet current of spectrometer 2 was set for the elastic peak and afterwards for +0.5% and -0.5% of the elastic momentum. This gave the shape of the elastic peak. The width of OR had been chosen large enough to ensure that these variations would not fall out of the flat-top region. All three values could be used for the cross-section calculation. To look for the tails in the elastic peak, values of ±5.5% and -6.5% of the peak current were set. An example of a momentum distribution measured in this way is shown in Fig.7. The line through the experimental points is a best-estimate curve. The broadening of the elastic peak by the finite dimensions of the slat counters has been unfolded (dashed line).

3.2.- Background subtraction.

The background was determined by drawing a straight line through the points above $\Delta p/p=+3.5\%$, which results in a weakly increasing background towards lower momenta (line (1) in Fig.7). When this background is subtracted the shape of the spectrum at the low-energy side is determined by the radiation effects and inelastic processes, i.e. π^+ and π^o production. These two processes could be separated in the following way: The beginning of the inelastic contribution was taken to be one half of the elastic peak halfwidth above the calculated

threshold, and the slope of the inelastic spectrum (line (2) in Fig.7) was chosen to yield the calculated radiation tail of the elastic peak. The slightly momentum depending background was typically 12%, the inelastic contribution was only 2% in the worst case.

From the analysed spectrum we thus obtained the ratio of the background to the whole counting rate for the range of the OR width. The ratio was then applied to the plateau value to find the elastic counting rate N^{St}.

This procedure was followed for both shower-counter discrimination levels, which were separated from each other by 6 to 9 db. Both results N^{St} agreed within the statistical uncertainty.

3.3.- The momentum acceptance of the counters.

Using the flat-top method, the width Δp of OR is not critical. Because of the background subtraction procedure it nevertheless enters the calculation. For spectrometer 2, for instance, the geometrical distance of the large counters multiplied by the calculated dispersion gave $\Delta p/p=6.80\%$, if multiplied by the measured dispersion gave $\Delta p/p=6.85\%$. The half width of OR was 6.7% and the integration of the elastic peak resulted in an effective $\Delta p/p=6.95\%$. The overall mean value was $\Delta p/p=(6.80\pm0.5)\%$. With the background being typically 12%, this uncertainty in $\Delta p/p$ introduces an uncertainty of 0.2% in N^{St}.

With the elastic rate N^{St} calculated from the flat-top method, an effective width Δp_{eff} for the slat counter was determined from

$$\Delta p_{eff} = \frac{\int N \cdot dp}{N^{St}} .$$

Especially at spectrometer 1 this area method of integrating the slat counter spectrum was used at very low counting rates, when a wide scraper slit had to be used to get a reasonable intensity on the target. Such a momentum spectrum at a cross section of $4 \cdot 10^{-35}$ cm^2/sterad is shown in Fig.8.

3.4.- The reference measurements.

For each setting of incident energy the recoil protons at $q^2=10\ f^{-2}$ were measured twice by spectrometer 2, once before and once after the electron measurements. Because of the large momentum variance of the protons across the spectrometer aperture, which could not entirely be adjusted by rotating the counter bank, this spectrum was broader than the electron spectra, see Fig.9. Nevertheless the analysis was simplified, because no important amount of inelastic processes was observed (only π^o production contributes), although the threshold is as close as about 1% to the elastic momentum.

The reduction procedure was essentially the same as with the electrons, but in addition the OR momentum distribution could be integrated. The net result of the different analyses agreed within 1-2%. The yield obtained at the beginning and at the end of an energy setting fluctuated a bit more, which was probably due to a change of the beam sweeping across the target. The greatest difference was typically 3%.

In order to obtain the best form factors for calculating the reference cross section, we fitted the values of Stanford [6] and Orsay[7] from $q^2=7$ to $q^2=13\ f^{-2}$ with a parabola. This gives at $q^2=10\ f^{-2}$ $G_E=0.407$ and also $G_M/\mu=0.407$[11]. The uncertainty in these form factors implies an uncertainty in the cross section of 3%, which is of the same order as the one in the bremsstrahlung cross section.

3.5.- Corrections.

Bremsstrahlung corrections. There are two bremsstrahlung processes which cause elastic events to fall out of the momentum acceptance of the spectrometer.

(i) Real bremsstrahlung of the scattered electrons while traversing the target and the foils of the vacuum chamber of the spectrometer. The total traversed thickness was $0.8\cdot10^{-3}$ radiation lengths, giving a correction factor of 1.003.

(ii) Bremsstrahlung in the scattering process, commonly called Schwinger effect. We used the formula calculated by Meister and Yennie[12], which resulted in a correction of typically 15% for the electron measurements and of 3% for the reference measurements of the recoil protons.

Proton collision losses. Before reaching the dE/dx counter the protons suffer collisions in the scintillation material of the counter bank. Cross sections for nuclear collision were taken form Carvalho[13] and Millburn et al.[14], who published measurements on proton absorption of 200 MeV protons, which is just the energy of the $q^2=10\ f^{-2}$ recoil protons. The measurements give an absorption cross section of 220 mbarn and a total nuclear elastic cross section of 80 mbarn. From the angular distribution we calculated that 40% of the protons which are elasticaly scattered in the scintillation material hit the dE/dx scintillator. The cross sections for both processes resulted in a total loss of (5.7±1.0)%.

Counting-rate losses due to multiple Coulomb scattering of the protons were negligible.

Bremsstrahlung from the target cup. The main reason to use the recoil protons as a normal was the fact that bremsstrahlung form the target cup causes too large a correction, particularly at low energy, where the beam entered the target only a few tenths of a millimeter (correction factor 1.40-1.60). At energies greater than 3 GeV the correction was always smaller than 1.15.
The correction was determined by measuring the amount of bremsstrahlung for a fixed number of circulating electrons as a function of the position of the horizontal scraper block[5]. By differentiation the distribution of the beam density j(r) on the target was derived, where r is the distance from the target center.
The part γ_H of the bremsstrahlung coming from hydrogen, is

$$\gamma_H = \int_{-R}^{+R} \frac{d_H(r)/x_H}{d_H(r)/x_H + d_F(r)/x_F} \cdot j(r) \cdot dr,$$

where $d_{H,F}$ is the target material of hydrogen and foil respectively as seen by the beam, and R is the target radius.

3.6.- Cross section calculation.

The electron-proton scattering cross section is given by

$$\frac{d\sigma}{d\Omega} = \frac{N^{St}}{N_e \cdot N_H \cdot d\Omega} f \ ,$$

where N^{St} denotes the yield of the elastically scattered electrons, N_H the number of target H-atoms and N_e the number of incident electrons; f is the product of the various correction factors f_i. Inserting Loschmidt's number N_L, the quantameter constant κ, and the hydrogen radiation length X_H=59.4 g/cm^2 one obtains

$$\frac{d\sigma}{d\Omega} = \frac{N^{St}}{N_L \cdot \kappa \cdot X_H \cdot E_o \cdot \gamma_H \cdot d\Omega} f \ ,$$

When relating this to the proton cross section the quantities κ, X_H, γ_H and the f_i due to the quantameter reading cancel, and the cross section is given by

$$\frac{d\sigma}{d\Omega} = \frac{N^{St}_{electr.}}{N^{St}_{prot.}} \frac{d\Omega_{prot.}}{d\Omega_{electr.}} \left(\frac{d\sigma}{d\Omega}\right)_{proton} \ ,$$

where $d\sigma/d\Omega_{proton}$ is the calculated proton cross section.
As an example of typical correction factors and uncertainties the the values for a cross section at q^2=60 f^{-2} are tabulated in TableI. Table II gives the corresponding values for a cross-section measurement of recoil protons a) using it for normalisation and b) when the measurement with the quantameter reading as a reference is used.

4.- Results.

4.1.- The differential cross sections.

The aim of this experiment was to measure cross sections at $q^2 = 39$, 60 and 80 f^{-2} at different angles in order to deduce the proton form factors. All cross sections obtained via detection of the scattered electrons are listed in Table III. The measurements at 16-22 f^{-2} served for testing the apparatus at the beginning of each run.

In Table IV the cross sections obtained via recoil protons are listed, which had been normalized against the quantameter.

4.2.- The form factor separation.

The form factors are extracted from the measured cross section according to the Rosenbluth formula

$$\frac{d\sigma}{d\Omega} = \sigma_{Mott} \cdot \tan^2\theta/2 \cdot \{\frac{G_E^2 + t\, G_M^2}{1 + t} \cot^2\theta/2 + 2t \cdot G_M^2\} \quad ,$$

where

$$\sigma_{Mott} = (\frac{e^2}{2E_o})^2 \cdot \frac{\cos^2\theta/2}{\sin^4\theta/2} \quad \frac{1}{1 + 2E_o/M \sin^2\theta/2}$$

and

$$t = q^2/4M^2.$$

The values $R = \frac{d\sigma/d\Omega}{\sigma_{Mott}} \cot^2\theta/2$ plotted versus $\cot^2\theta/2$ for fixed momentum transfer should follow a straight line, the ordinate value at $\cot^2\theta/2 = 0$ giving G_M^2 and the slope giving the linear combination $G_E^2 + tG_M^2$.

Actually the experimental points were not taken at exactly the same value of the momentum transfer, due to a slight variation in the energy setting of the synchrotron. Therefore the values of R had been shifted to the common integer value parallel to the line of

R, which had been calculated for the fixed angle from $G_E=G_M/\mu=\left(\frac{1}{1+q^2/0.71GeV^2}\right)^2$. This shifting did not change R more than 5% andintroduced an error into R of less than 1%, which results from the hypothetical from-factor curve.
The experimental values R, partly combined with data from other groups, are fitted to a straight line by the least-square method. The obtained form factors are summarized in Table V. The errors in the form factors are the weighted errors of the cross sections, the goodness of the fit to the straight line is indicated by the χ^2.

The cross sections from the test measurements at $q^2= 20, 22\ f^{-2}$ (spectrometer 1) and $q^2=16, 17\ f^{-2}$ (spectrometer 2) do agree well with the Rosenbluth straight line calculated from the Stanford data[6]. Two examples are shown in Fig. 10, the straight lines are evaluated from Janssens' three-pole fit.
As a justification of our normalisation method the straight line for $q^2=10\ f^{-2}$ is shown in Fig. 11. These cross sections are normalized against the quantameter. The straight line represents $G_E=G_M/\mu=0.407$ as obtained from the parabola fit (see 3.4.). No deviation from the Rosenbluth straight line has been found, in contrast to the measurements by the Harvard group, reference (3) page 49/50. When all available data for this point are combined, the form factors turn out to be $G_E=0.408$ and $G_M/\mu=0.404$ with a $\chi^2=8.0$ for 14 degrees of freedom.
The Rosenbluth plots of the measurements at $q^2= 39, 60$ and $80\ f^{-2}$ are shown in Fig. 12. No violation of the Rosenbluth formula is observed. For the straight line at $q^2=39\ f^{-2}$ we combined our data with those from Albrecht et al.[15] and Bartel et al.[16], the last one shifted from $q^2=40\ f^{-2}$ to $q^2=39\ f^{-2}$. The over-all χ^2 is 8.0 for 8 degrees of freedom. If one takes in addition the data from Berkelman et al.[17], also shifted from 40 to $39\ f^{-2}$, the form factors do not change appreciably, but the χ^2 goes up to 18.6 for 11 degrees of freedom. When only data from this experiment are used an imaginary G_E is abtained. At $q^2= 60$ and $80\ f^{-2}$ only data from this

experiment are used, giving $\chi^2=25$ for six degrees of freedom and $\chi^2=1.6$ for one degree of freedom respectively.

Form the cross section at $q^2=110\ f^{-2}$ the magnetic form factor was calculated using the assumption $G_E=G_M/\mu$. This is justified by the fact that at these kinematic conditions the electric scattering contributes only around 5% to the cross section. In addition data from Albrecht et al.[15] and Bartel et al.[16] for the straight line fit were used.

The form factors are plotted logarithmically in Fig. 13 and Fig.14. The dashed line in the figure for G_E is a smoothed curve to the experimental value of G_M/μ, where the smoothing was accomplished by taking at least six points in the neighbourhood and fitting them with a parabola $y=a+bq^2+cq^4$. It seems that the relation $G_E=G_M/\mu$ empirically valid in the region of low momentum transfer continues to hold, however,it must be pointed out that the electric form factor is highly sensitive to the cross sections at high momentum transfer. Even the estimation of the errors in the cross section enters the value of G_E.

5.- Conclusions.

In the present experiment elastic electron-proton cross sections were measured at momentum transfers of $q^2=$ 39, 60 and 80 f^{-2} with an accuracy of 6-15%, the overall systematic error was estimated to be 6%. As a reference, cross sections of the elastic scattering were taken at $q^2=10\ f^{-2}$, where the Rosenbluth formula has been shown to hold up to 6 GeV primary energy. At low momentum transfer the cross sections agree well with those extrapolated from the Stanford data.

No deviation from the Rosenbluth formula has been observed at high momentum transfer up to 80 f^{-2}. The formula yields real value for the electric form factor, which seems to be equal to the magnetic form factor normalised to one at zero momentum transfer. Nevertheless it must be emphasized that the extraction of G_E is highly sensitive to the cross section in this region of high momentum transfer.

* * *

The authors are indebted to Professor Jentschke for his persistent interest in this work and thank many people for their indispensable support and encouragement to the experiment.

In particular we thank the synchrotron staff of DESY. Further we are indebted to E. Dasskowski for the construction and the final assembling of the carriages. It is a pleasure to thank Dr. H. Pingel for designing and constructing the liquid hydrogen target and K. M. Thiele for reliably operating it. S.K. Tsoi we thank for his help in taking the recoil proton data.

Table I.-

Summary of typical correction factors and uncertainties.

$q^2=60\ f^{-2}$ $\theta=32^{\circ}$ $E_o=3.50$ GeV

Source	Correction factors for cross sections	Error in cross section (%)
1) Counter efficiencies		
Momentum def. counters	1.000	0.5
Cerenkov counter	1.007	0.3
Shower counter level 1	1.029	0.8
level 2	1.015	0.8
2) Dead time level 1	1.018	0.8
level 2	1.018	0.8
3) Radiative corrections		
Yennie formula	1.195	2.0
Loss at spectrometer entrance foils	1.003	0.0
4) Data analysis, background subtraction method	1.000	1.5
5) Primary energy	1.000	1.5
6) Solid angle	0.976	0.5
7) Scattering angle	1.000	0.5
8) Stability of integrator device	1.000	0.3
9) Counting statistics	1.000	4.2
10) Reference cross section at $q^2=10\ f^{-2}$	1.066	3.9
Total	1.312	6.7%

Table II.-

Summary of typical correction factors and uncertainties for proton measurements

a) when used as normalisation

b) when the quantameter is used as normal.

$q^2 = 10\ f^{-2}$ $\quad \phi_p = 66.36^\circ$ $\quad E_o = 3.50$ GeV

Source	Correction factors for cross section	Error in cross section (%)
1) Counter efficiencies		
Momentum def. counters	1.000	0.3
Proton dE/dx counter	1.000	0.3
2) Dead time	1.004	0.5
3) Radiative corrections		
Yennie formula	1.024	1.0
4) Data analysis, background subtraction method	1.000	1.5
5) Collision loss	1.060	1.0
6) Primary energy	1.000	0.5
7) Solid angle	0.976	1.0
8) Scattering angle	1.000	0.5
9) Cross section calculated from G_E=0.407, G_M/μ=0.407	1.000	3.0
a) Total for reference cross section	1.064	3.9%
9') Quantameter		
Radiation from target foil	1.129	3.0
Non asymptotic bremsstrahlung	0.994	0.0
Bremsstrahlung loss in quantameter	0.970	1.0
Integrator calibration, integrator stability	0.986	0.5
Quantameter constant	1.000	3.0
Radiation length	1.000	3.0
b) Total with quantameter	1.142	6.0%

Table III.- Electron-proton elastic scattering cross sections.

q^2 (f^{-2})	E_o (GeV)	θ	$\frac{d\sigma}{d\Omega}$ (10^{-34} cm^2/sterad)	$\Delta\left(\frac{d\sigma}{d\Omega}\right)$(%)	$R = \left(\frac{d\sigma}{d\Omega}/\sigma_{Mott}\right)\cot^2\theta/2$
16	1.52	34.14°	368	5.7	1.81 ± 0.11
17	1.68	31.71°	389	6.2	1.99 ± 0.13
20	1.19	55.00°	69.2	8.5	0.616 ± 0.053
22	1.25	55.10°	55.1	5.6	0.564 ± 0.032
39	2.71	31.55°	31.8	12.3	0.473 ± 0.057
	2.71	31.55°	30.2	5.8	0.450 ± 0.026
	2.25	40.04°	16.3	7.8	0.291 ± 0.023
	1.87	51.82°	9.87	7.1	0.224 ± 0.016
	1.71	59.80°	6.43	5.9	0.171 ± 0.010
	1.70	59.91°	5.69	8.2	0.151 ± 0.013
	1.52	72.68°	4.13	6.1	0.139 ± 0.008
	1.52	72.68°	4.42	6.7	0.148 ± 0.010
60	3.46	32.11°	6.14	6.7	0.169 ± 0.012
	2.67	46.06°	2.41	6.5	0.095 ± 0.0062
	2.63	47.10°	2.43	10.8	0.099 ± 0.011
	2.22	62.50°	0.936	10.7	0.0547± 0.0059
	2.22	62.78°	0.875	6.2	0.0513± 0.0032
	1.88	88.87°	0.619	8.3	0.0613± 0.0052
	1.87	90.00°	0.406	11.1	0.0411± 0.0046
	1.67	128.90°	0.239	15.8	0.0411± 0.0065
80	4.12	32.18°	1.99	8.5	0.0838± 0.0072
	3.47	41.17°	0.890	8.1	0.0491± 0.0040
	2.67	65.23°	0.282	11.4	0.0299± 0.0034
110	8.46	61.49	0.0887	12.4	0.0157± 0.0020

Table IV.- Electron-proton elastic scattering cross sections at $q^2=10\ f^{-2}$, measured via recoil protons and normalised with a quantameter.

E_o	ϕ_p	$\frac{d\sigma}{d\Omega}$ ($10^{-32}cm^2$/sterad)	$\Delta\frac{d\sigma}{d\Omega}$ (%)	$R=\frac{d\sigma/d\Omega}{\sigma_{Mott}}\cot^2\theta/2$
2.71	64.89°	74.1	7.2	16.41 ± 1.2
3.46	66.36°	147.8	6.1	31.41 ± 2.0
4.25	67.34	219.0	6.0	45.46 ± 2.8
6.06	68.63	363.0	5.0	105.6 ± 5.3

Table V.- ELECTRIC AND MAGNETIC FORM FACTORS

q^2		G_E	ΔG_E	G_M/μ	$\Delta G_M/\mu$	χ^2	Number of cross sections and source
f^{-2}	$(GeV/c)^2$						
10	0.390	0.408	+0.007 -0.009	0.404	±0.005	8.0	4 this report + 7 ref. 6) + 2 ref.7) + 1 ref.5) + 1 ref.15) + 1 ref. 16)
16	0.623	0.275	+0.017 -0.018	0.281	±0.005	3.2	1 this report + 6 ref. 6) + 1 ref. 5)
17	0.662	0.251	+0.022 -0.024	0.275	±0.007	1.2	1 this report + 3 ref. 6) + 1 ref.15)
20	0.778	0.215	+0.009 -0.009	0.233	±0.004	19.4	1 this report + 6 ref. 6) + 2 ref.15) 3 ref. 16)
22	0.856	0.187	+0.024 -0.028	0.223	±0.004	5.3	1 this report + 4 ref. 6) + 1 ref. 5)
39	1.519	0.088	+0.018 -0.022	0.106	±0.004	8.0	8 this report + 1 ref.15) + 1 ref.16)
39	1.519	0.087	+0.012 -0.014	0.107	±0.002	18.6	8 this report + 1 ref.15) + 1 ref.16) + 3 ref. 17)
60	2.32	0.035	+0.028 -0.035	0.056	±0.003	25.2	8 this report
80	3.11	0.042	+0.031 -0.042	0.034	±0.005	1.6	3 this report
105	4.09	0.023	+0.014 -0.023	0.022	±0.0014	2.6	1 this report (q^2=110 f^{-2} shifted to 105 f^{-2}) + 3 ref. 14) + 1 ref. 15)
110	4.28	$G_E = G_M/\mu$ for analysis		0.022	±0.0013		1 this report

References and footnotes

(1) R. Hofstadter: Nuclear and Nucleon Structure, Benjamin Inc., N.Y. (1963).

(2) L.N. Hand, G.G. Miller and R. Wilson: Electric and Magnetic Form Factors, Rev. Mod. Phys., 35, 335 (1963).

(3) R. Wilson: Review of Nucleon Form Factors, Proceedings of the International Symposium on Electron and Photon Interactions at High Energies, Vol.I, Hamburg (1965).

(4) M. Rosenbluth: Phys. Rev., 79, 615 (1950).

(5) K.W. Chen, J.R. Dunning, A.A. Cone, N.F. Ramsay, J.K. Walker and R. Wilson: Phys. Rev., 141, 1267 (1966).

(6) T. Janssens, E.B. Hughes, M.R. Yearian, R. Hofstadter: Phys. Rev., 142, 922 (1966).

(7) B. Dudelzak: Thesis, Paris (1965), also
B. Dudelzak, A. Isakov, P. Lehmann, R. Tchapoutian: Proceedings of the XII International Conference on High Energy Physics at Dubna, Vol.I, 916 (1964).

(8) G. Lutz, H.D. Schulz, U. Timm and W. Zimmermann: DESY Internal Report F 33/3 (1966).

(9) L. Hand, I. Rees, W. Schlaer, J.K. Walker and R. Wilson: Nucleon Structure, Proceedings of the International Conference at Stanford, 364, (1963).

(10) R.R. Wilson: Nucl. Instr., 1, 101 (1957).

(11) For comparison: The three-pole fit in ref.(6) yields $G_E=0.410$ and $G_M/\mu=0.402$.

(12) N. Meister and D.R. Yennie: Phys. Rev., 130, 1210 (1963).

(13) H.G. de Carvalho: Phys. Rev., 96, 398 (1954).

(14) G.P. Millburn, W. Birnbaum, W.E. Crandall and L. Schecter: Phys. Rev., 95, 1268 (1954).

(15) W.Albrecht, H.J. Behrend, F.W. Brasse, W. Flauger, H. Hultschig and K.G. Steffen: submitted to Phys. Rev. Lett.

(16) W. Bartel, B. Dudelzak, H. Krehbiel, J.M. McElroy, U. Meyer-Berkhout, R.J. Morrison, H. Nguyen-Ngoc, W. Schmidt and G. Weber: Phys. Rev. Lett., 17, 608 (1966).

(17) K. Berkelman, M. Feldman, R.M. Littauer, G. Rouse and R.R. Wilson: Phys. Rev., 130 2061 (1963).

Figure captions.

Fig.1.- Plan view of the experimental arrangement.

Fig.2.- Schematic diagram for the spectrometer set-up.

Fig.3.- Pulse-height distribution of the Čerenkov counter.

Fig.4.- Pulse-height distribution of the shower counter at $q^2=39\ f^{-2}$, $E_o=1.9$ GeV, $\theta=52^\circ$.

Fig.5.- Two-dimensional plot of shower-counter pulses versus Čerenkov counter pulses showing their correlation. Dashed lines: events within this area are subtracted in the corresponding one-dimensional spectra.

Fig.6.- Momentum distribution of elastically scattered electrons at a high counting rate: $q^2=16\ f^{-2}$, $E_o=1.52$ GeV, $\theta=34.1^\circ$ taken with spectrometer 2. The spectrum measured with the crossed coincidence (upper curve) showes the flat top, whereas the unfolded spectrum of the slat counters (lower curve) shows the actual resolution of the spectrometer.

Fig.7.- Momentum distribution of elastically scattered electrons of $q^2=80\ f^{-2}$, $E_o=4.1$ GeV, $\theta=32^\circ$, taken with spectrometer 2.

Fig.8.- Momentum spectrum of elastically scattered electrons at a low counting rate: $q^2=60\ f^{-2}$, $E_o=1.87$ GeV, $\theta=90^\circ$, taken with spectrometer 1.

Fig.9.- Momentum spectrum of recoil protons at $q^2=10\ f^{-2}$, $E_o=6.1$ GeV, $\phi=68.6^\circ$, taken at spectrometer 2.

Fig.10.- Rosenbluth plot for $q^2=17\ f^{-2}$ and $22\ f^{-2}$. The straight lines are drawn according to the three-pole fit of reference (6).

Fig.11.- Rosenbluth plot for $q^2=10\ f^{-2}$, with the cross sections of this work normalized against the bremsstrahlung cross section. The straight line is drawn with $G_E=G_M/\mu=0.407$.

Fig.12.- Rosenbluth plots for $q^2=$ 39, 60 and 80 f^{-2}. The straight lines are the best fit by the least-sqares method.

Fig.14.- The electric form factor G_E versus q^2. The dashed line is a smoothed curve of G_M/μ.

Fig.13.- The magnetic form factor G_M/μ.

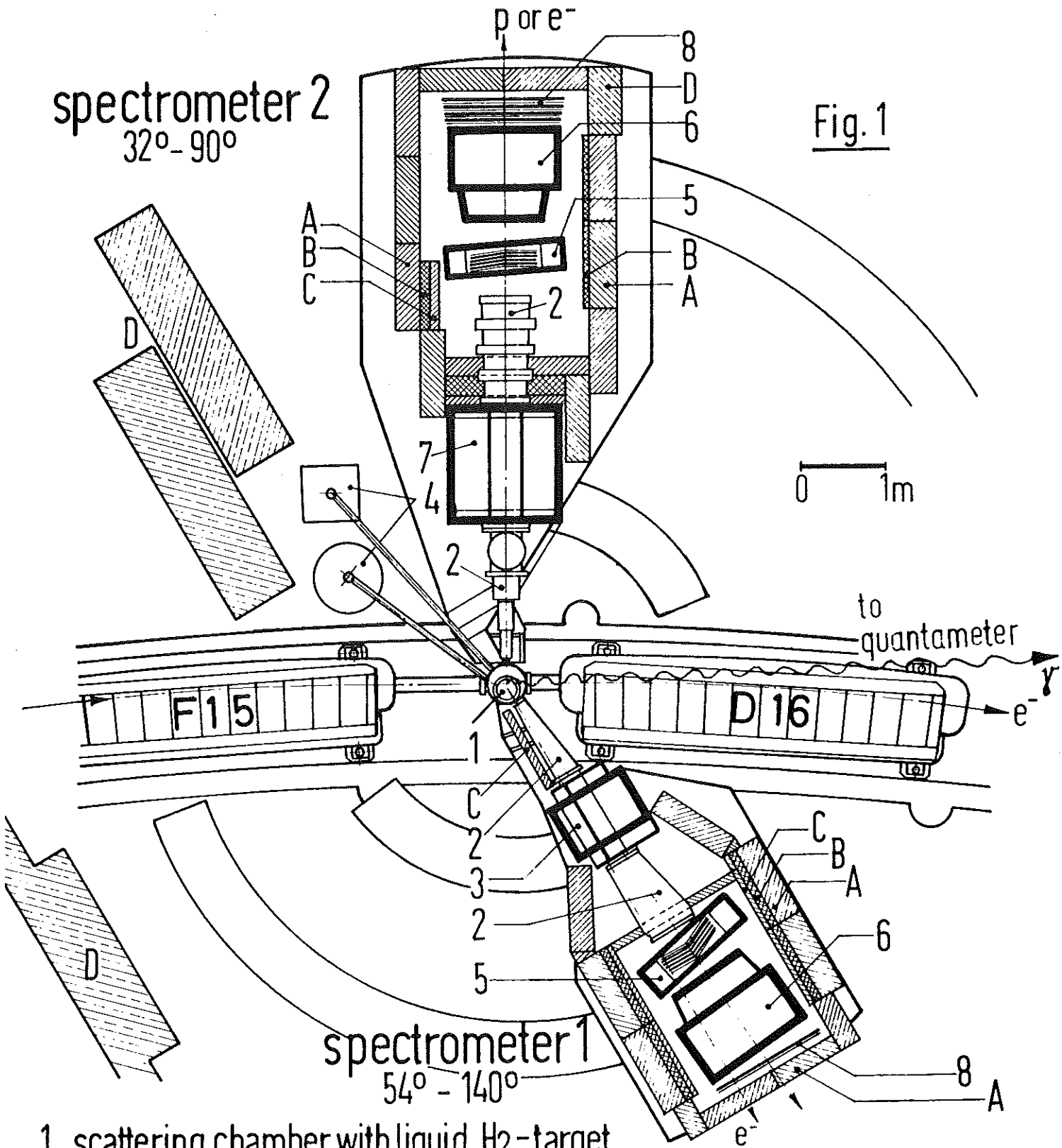

Fig. 1

1 scattering chamber with liquid H_2-target
2 vakuum chamber with entrance slits
3 halved quadrupole magnet $QC/2$
4 target supply and He-dewar
5 scintillation counters
6 gas-Čerenkov-counter (threshold)
7 quadrupole magnet QA
8 shower counter

shielding

A iron blocks
B $B_4C - CH_2$ - plates + paraffine
C lead blocks
D concrete blocks

e^--p-scattering at internal H_2-target

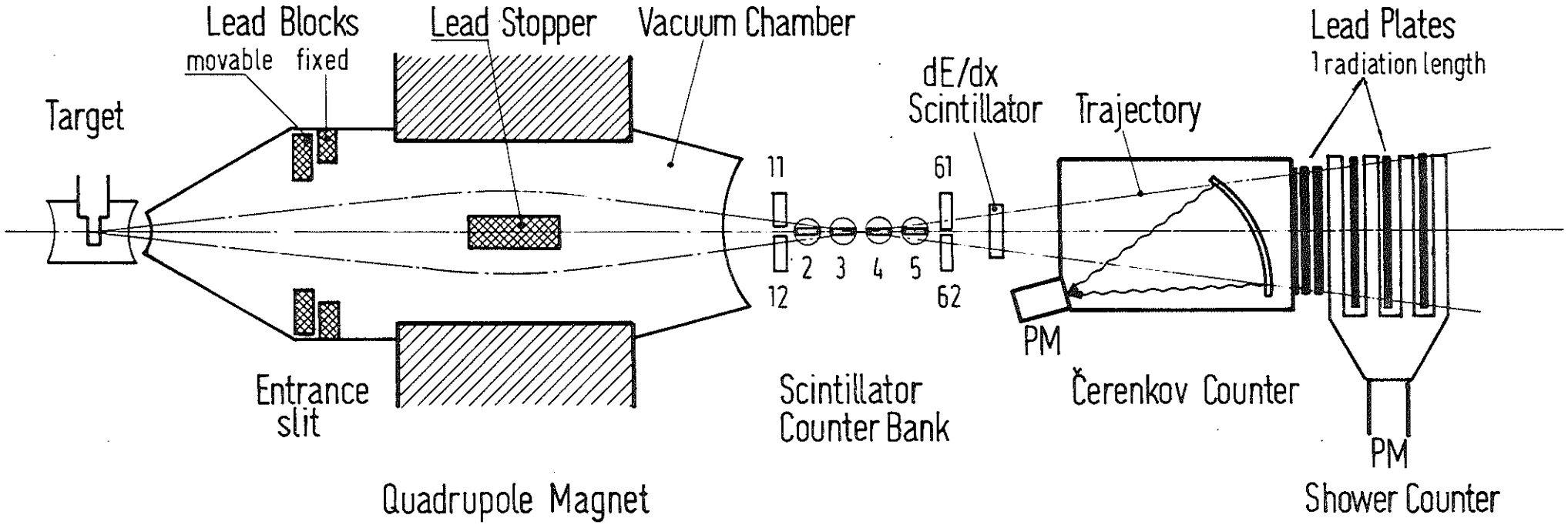
Lead Blocks
movable
fixed
Lead Stopper
Vacuum Chamber
Lead Plates
1 radiation length
Target
dE/dx
Scintillator
Trajectory
11
61
2
3
4
5
12
62
PM
Entrance
slit
Scintillator
Counter Bank
Čerenkov Counter
PM
Quadrupole Magnet
Shower Counter

Fig.2

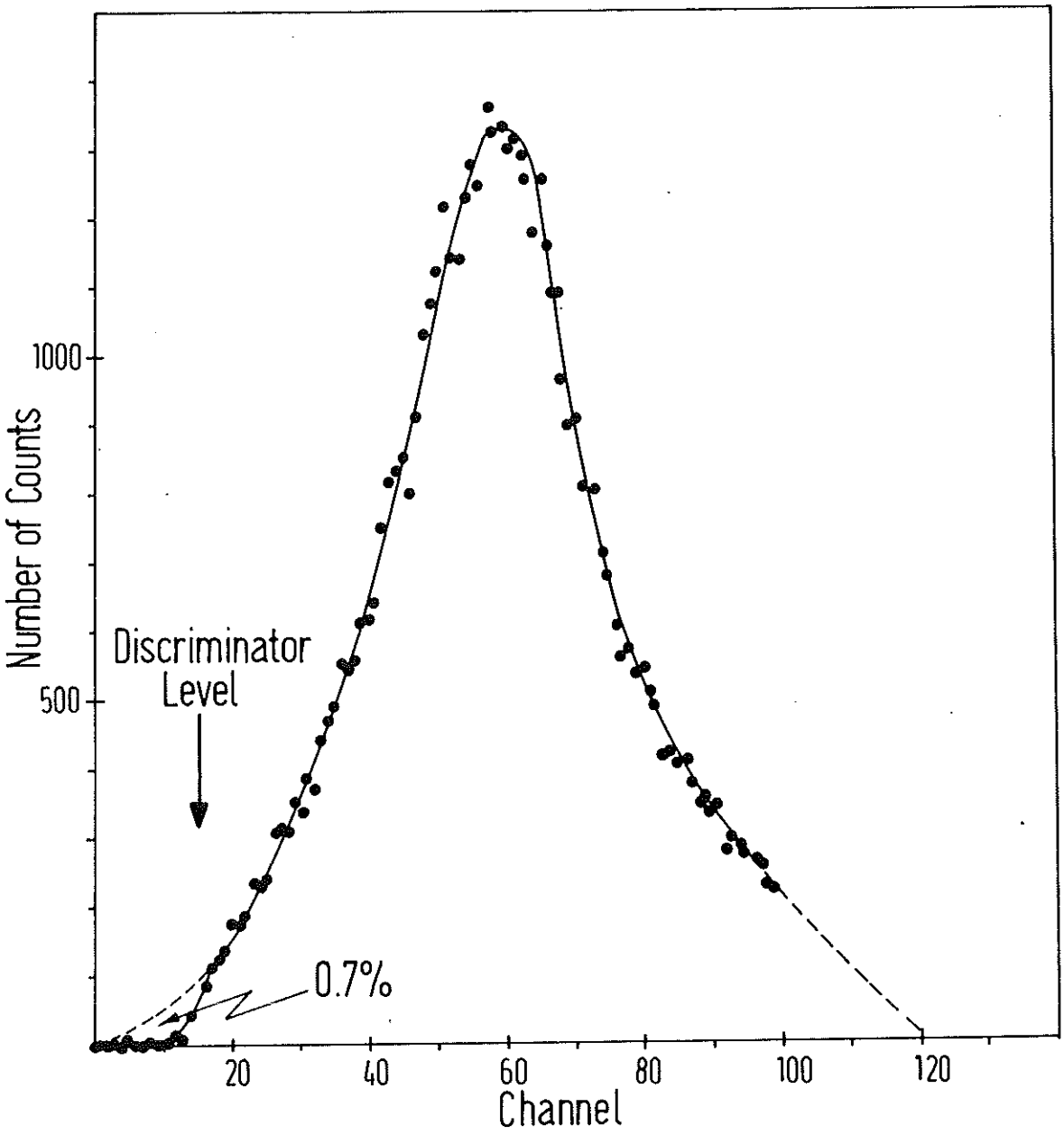
Number of Counts
1000
500
Discriminator
Level
0.7%
20
40
60
80
100
120
Channel

Fig. 3

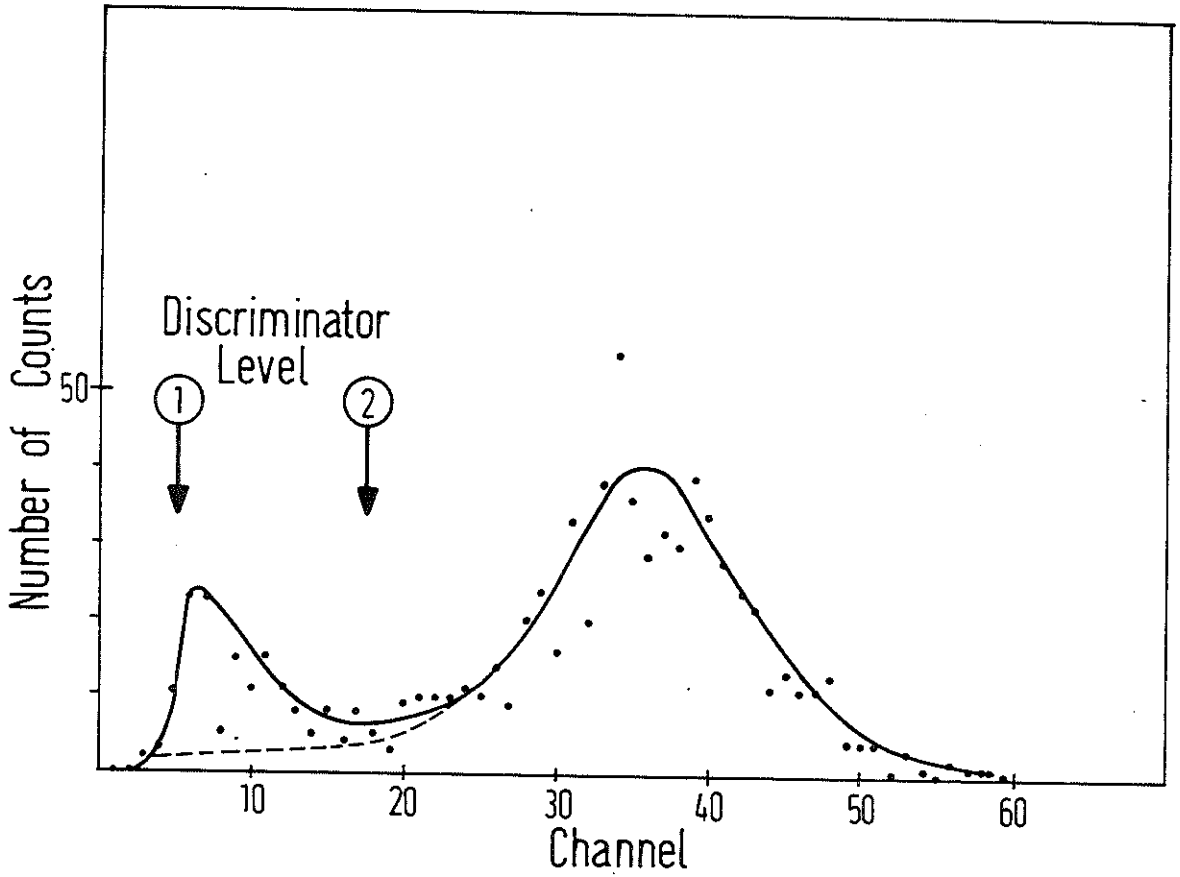
Number of Counts
50
Discriminator
Level
1
2
10
20
30
40
50
60
Channel

Fig. 4

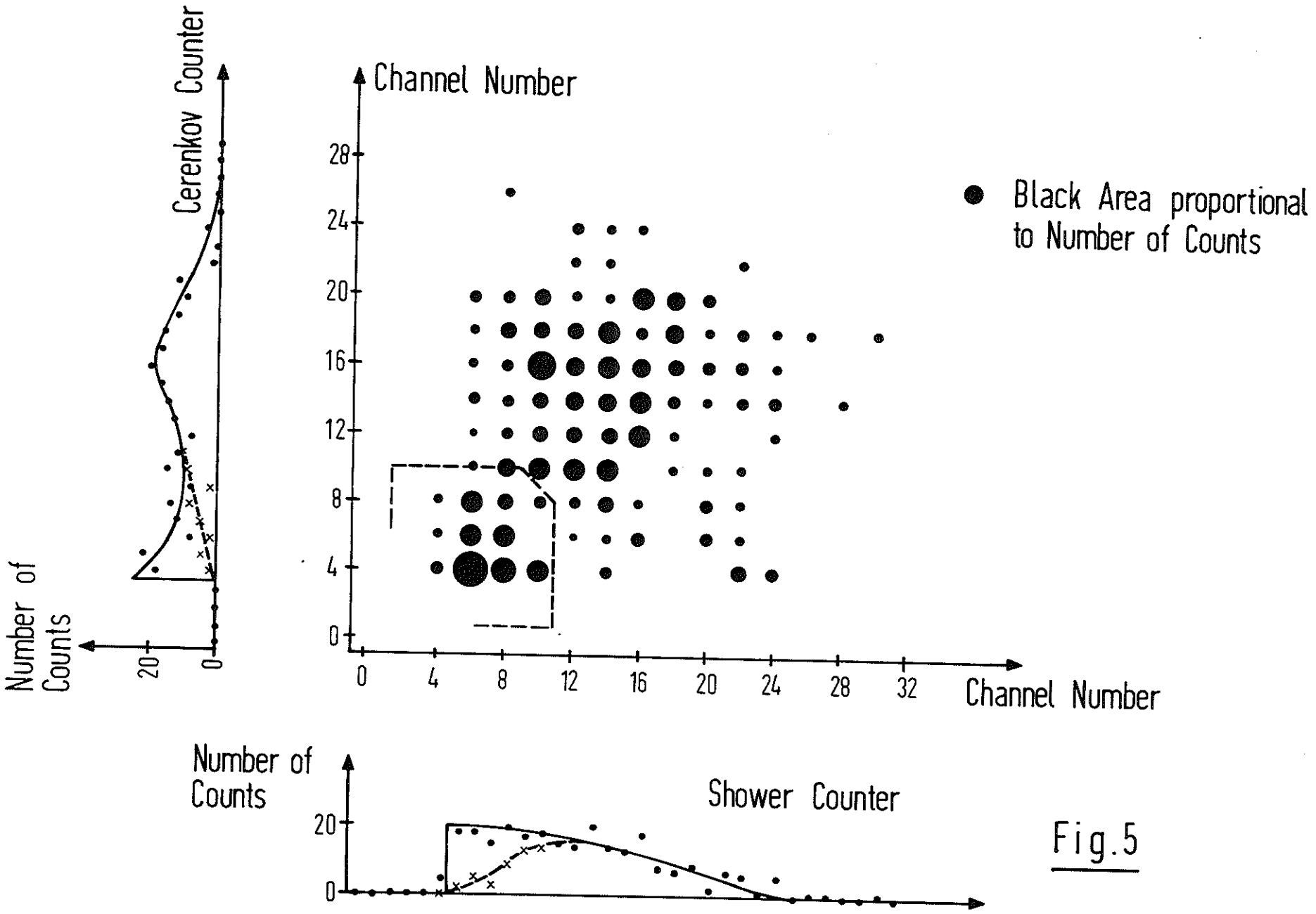
Cerenkov Counter
Number of Counts
20
0
Channel Number
28
24
20
16
12
8
4
0
0
4
8
12
16
20
24
28
32
Channel Number
Black Area proportional to Number of Counts
Number of Counts
20
0
Shower Counter

Fig.5

Fig.6

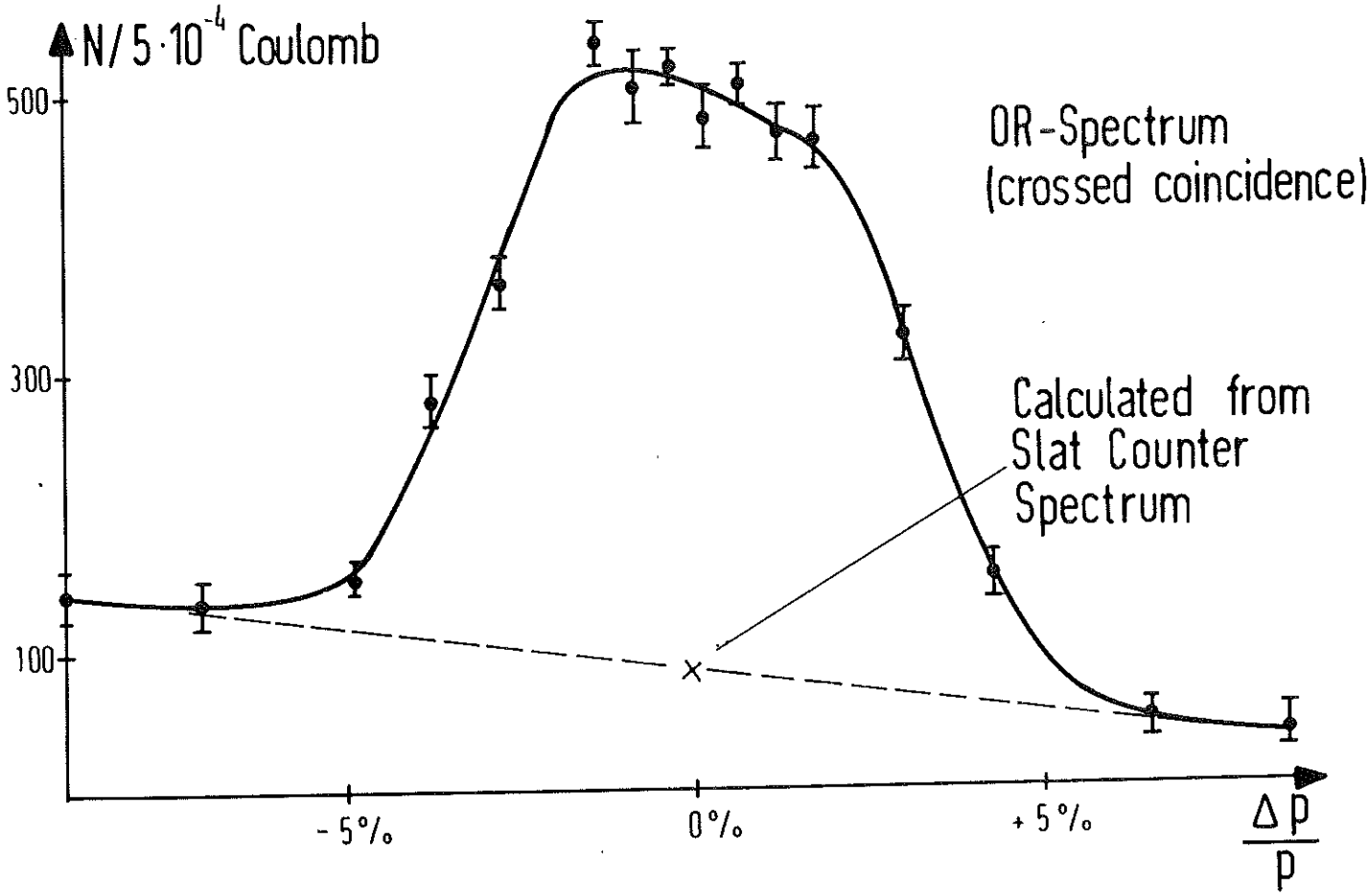
N/5·10⁻⁴ Coulomb
500
300
100
OR-Spectrum
(crossed coincidence)
Calculated from
Slat Counter
Spectrum
- 5%
0%
+ 5%
Δp/p

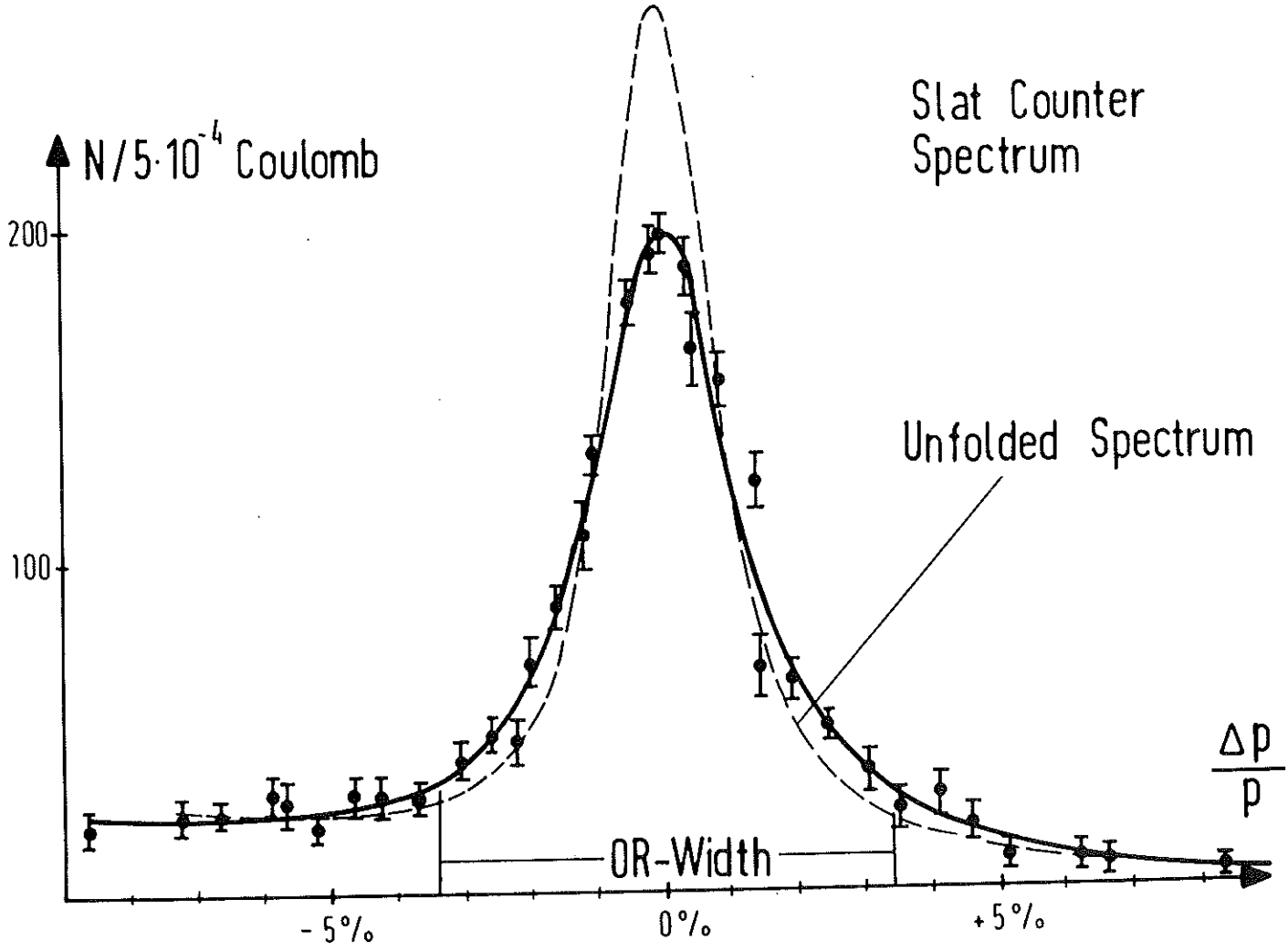
N/5·10⁻⁴ Coulomb
200
100
Slat Counter
Spectrum
Unfolded Spectrum
OR-Width
- 5%
0%
+ 5%
Δp/p

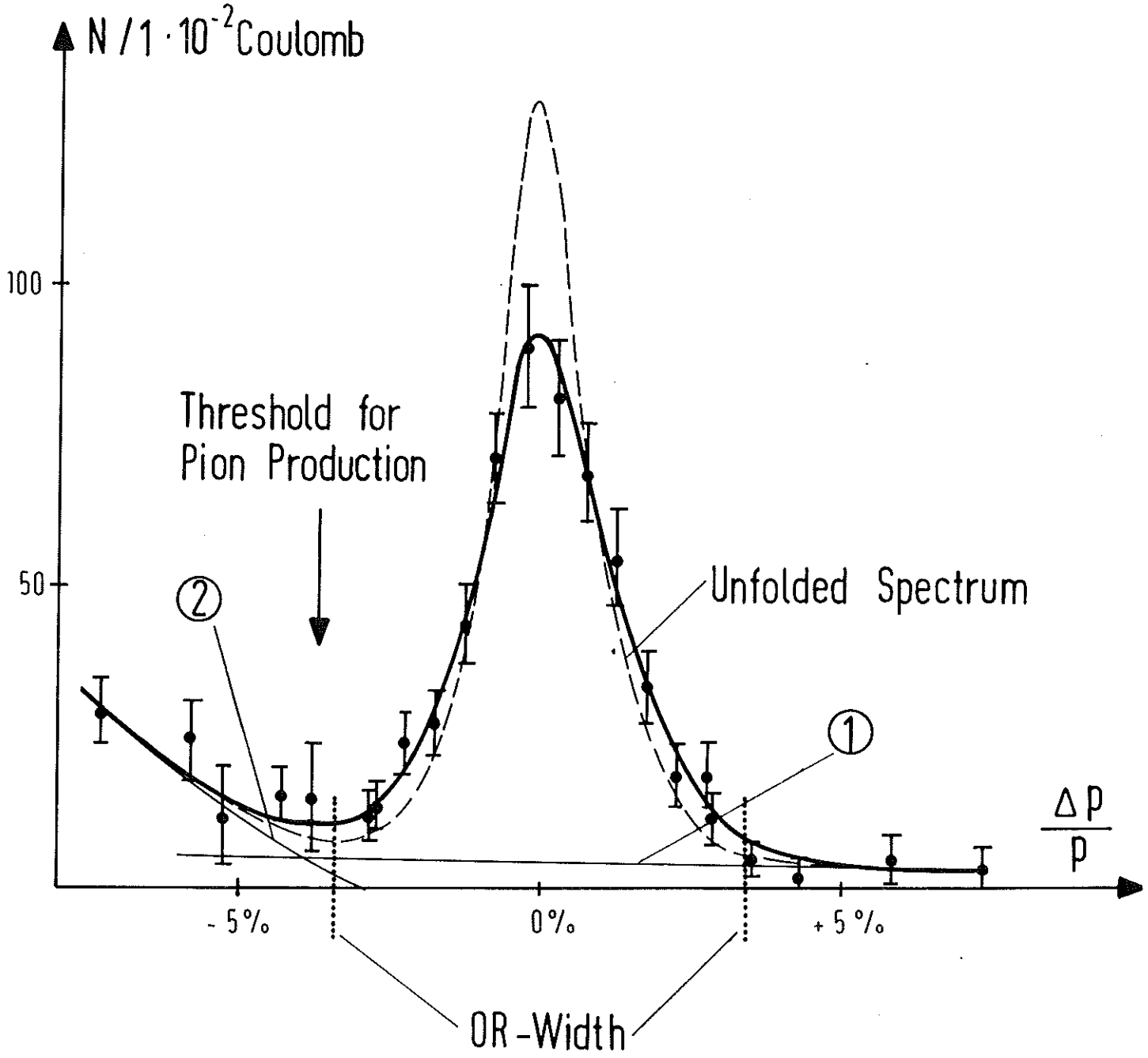
N / 1 · 10⁻² Coulomb
100
50
Threshold for
Pion Production
②
Unfolded Spectrum
①
Δp/p
- 5%
0%
+ 5%
OR-Width

Fig.7

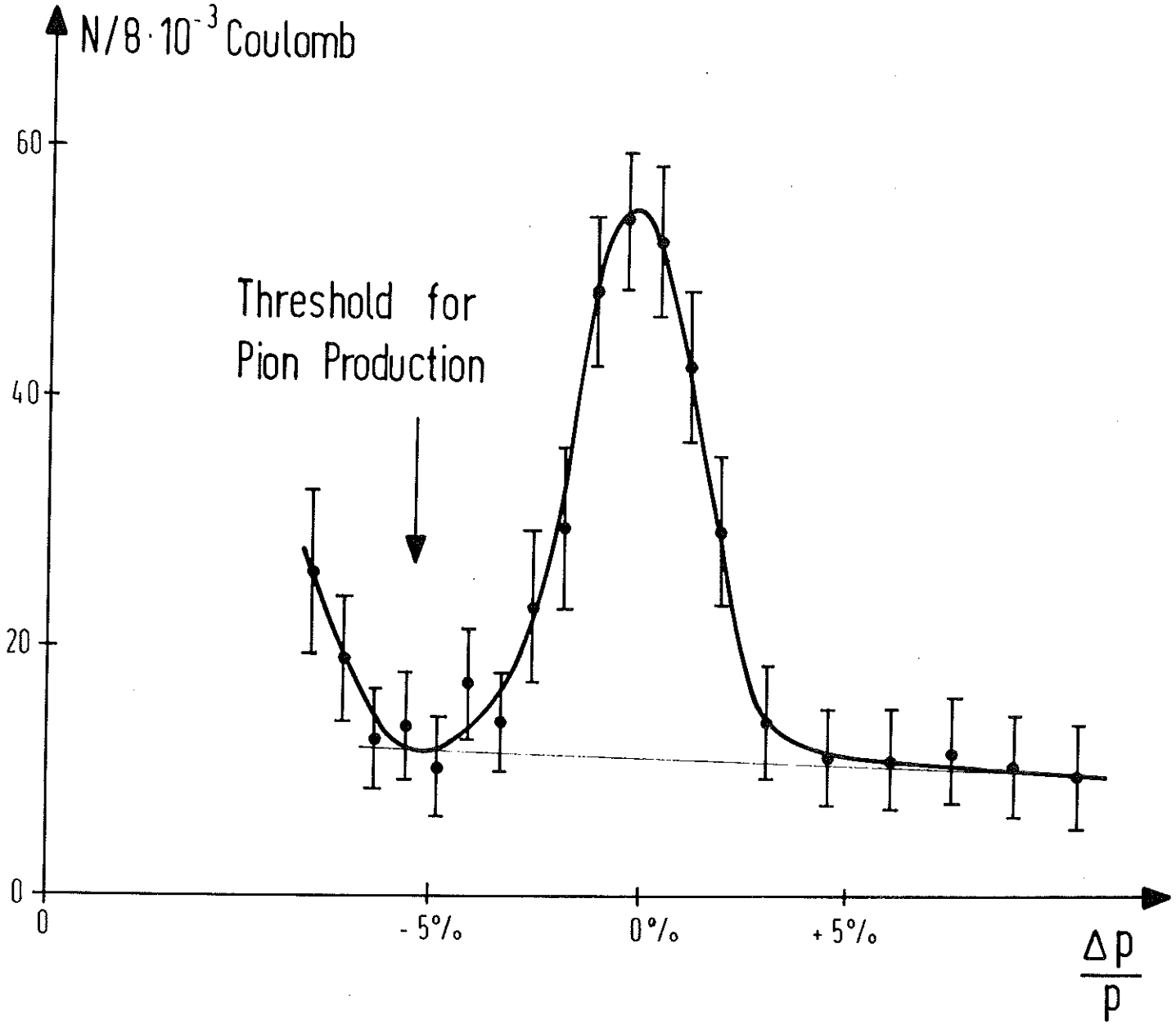
N/8·10⁻³ Coulomb
60
40
20
0
Threshold for
Pion Production
0
- 5%
0%
+ 5%
Δp
p

Fig. 8

Fig.9

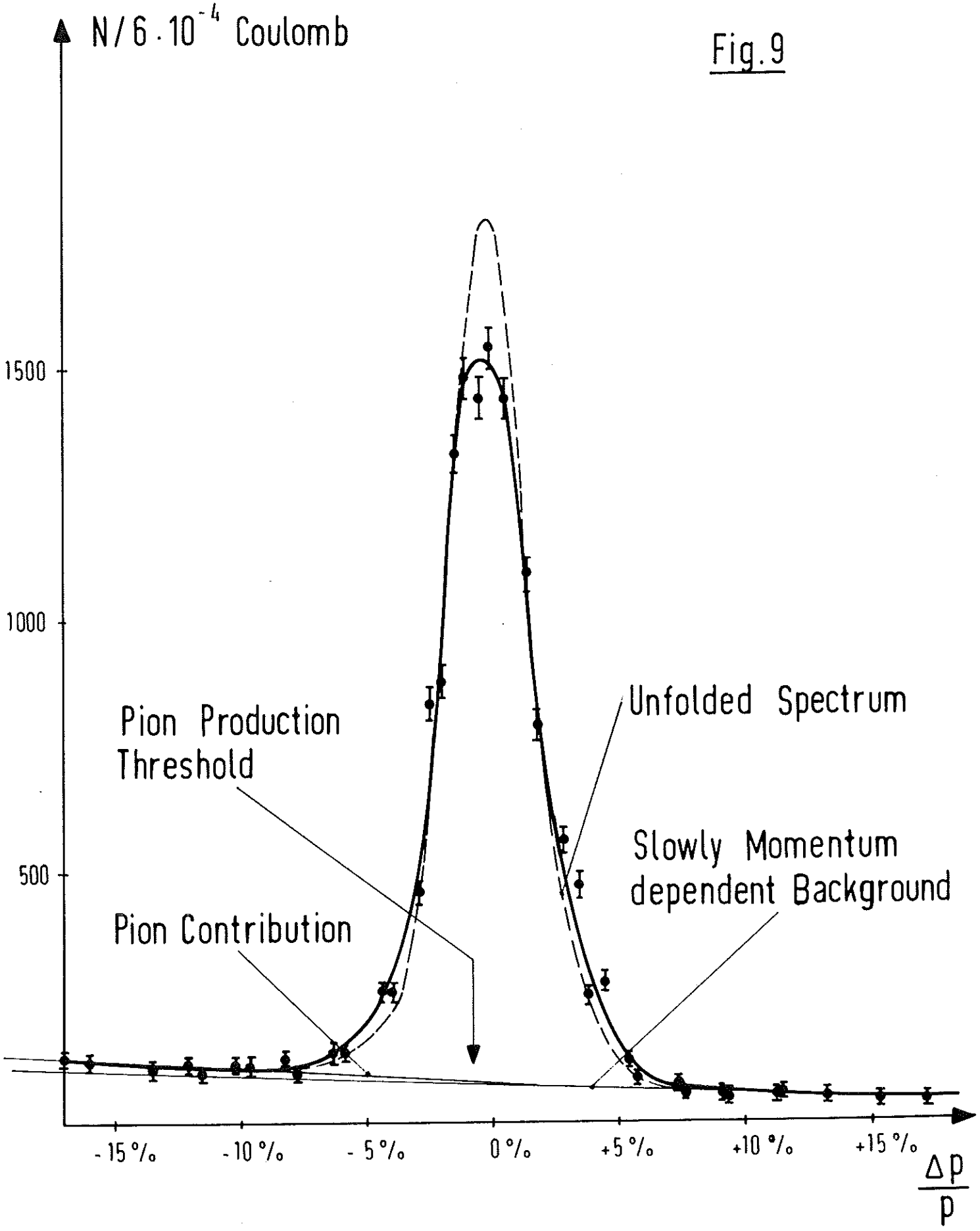
N/6·10⁻⁴ Coulomb
1500
1000
500
Pion Production Threshold
Unfolded Spectrum
Slowly Momentum dependent Background
Pion Contribution
-15 %
-10 %
-5 %
0 %
+5 %
+10 %
+15 %
Δp/p

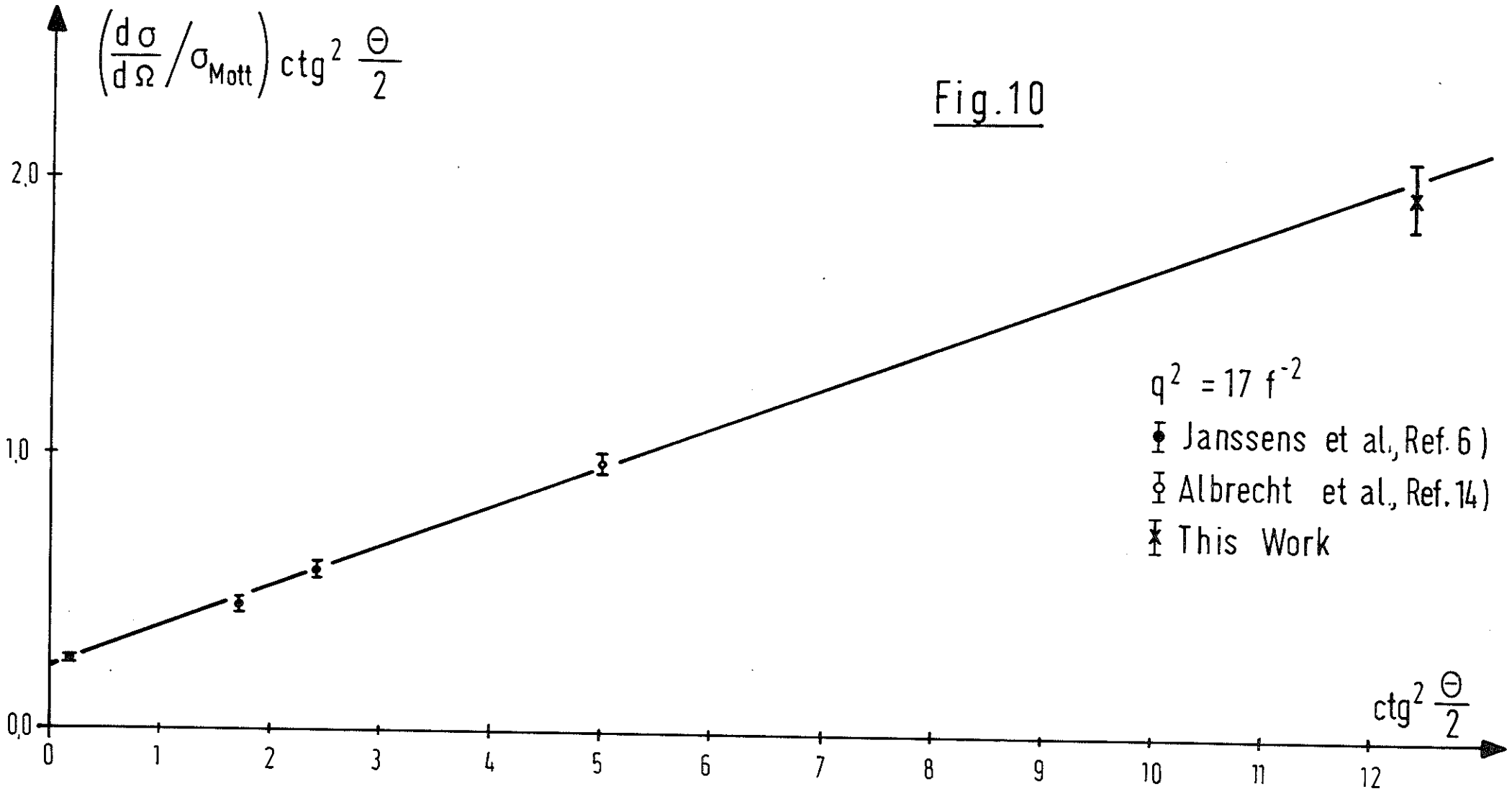
$\left(\frac{d\sigma}{d\Omega}/\sigma_{Mott}\right) ctg^2 \frac{\Theta}{2}$
2,0
1,0
0,0
0
1
2
3
4
5
6
7
8
9
10
11
12
$ctg^2 \frac{\Theta}{2}$
$q^2 = 17\ f^{-2}$
Janssens et al., Ref. 6)
Albrecht et al., Ref. 14)
This Work

Fig. 10

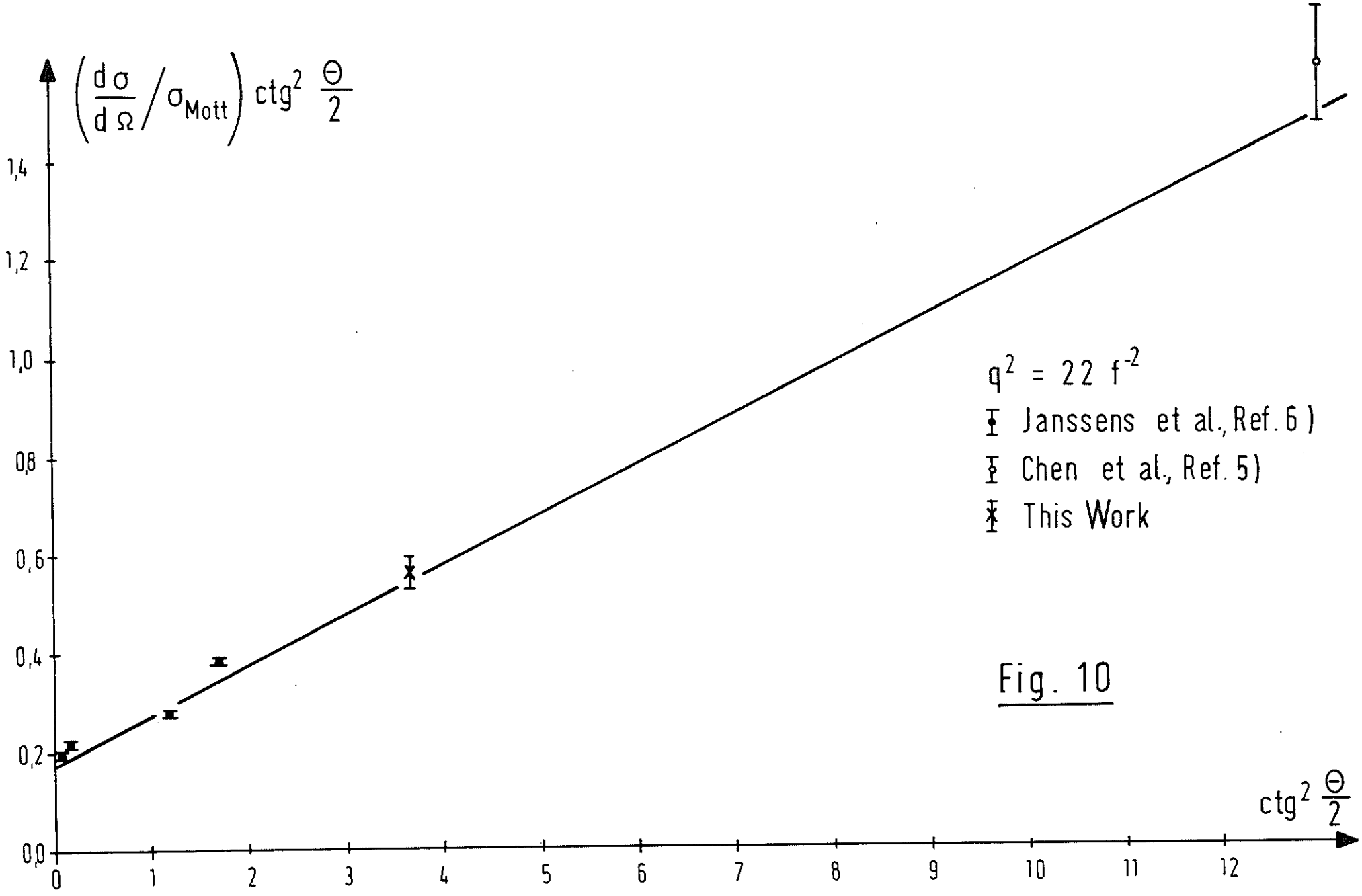
$\left(\frac{d\sigma}{d\Omega}/\sigma_{Mott}\right) ctg^2 \frac{\Theta}{2}$
1,4
1,2
1,0
0,8
0,6
0,4
0,2
0,0
0
1
2
3
4
5
6
7
8
9
10
11
12
$ctg^2 \frac{\Theta}{2}$
$q^2 = 22\ f^{-2}$
Janssens et al., Ref. 6)
Chen et al., Ref. 5)
This Work

Fig. 10

Fig. 11

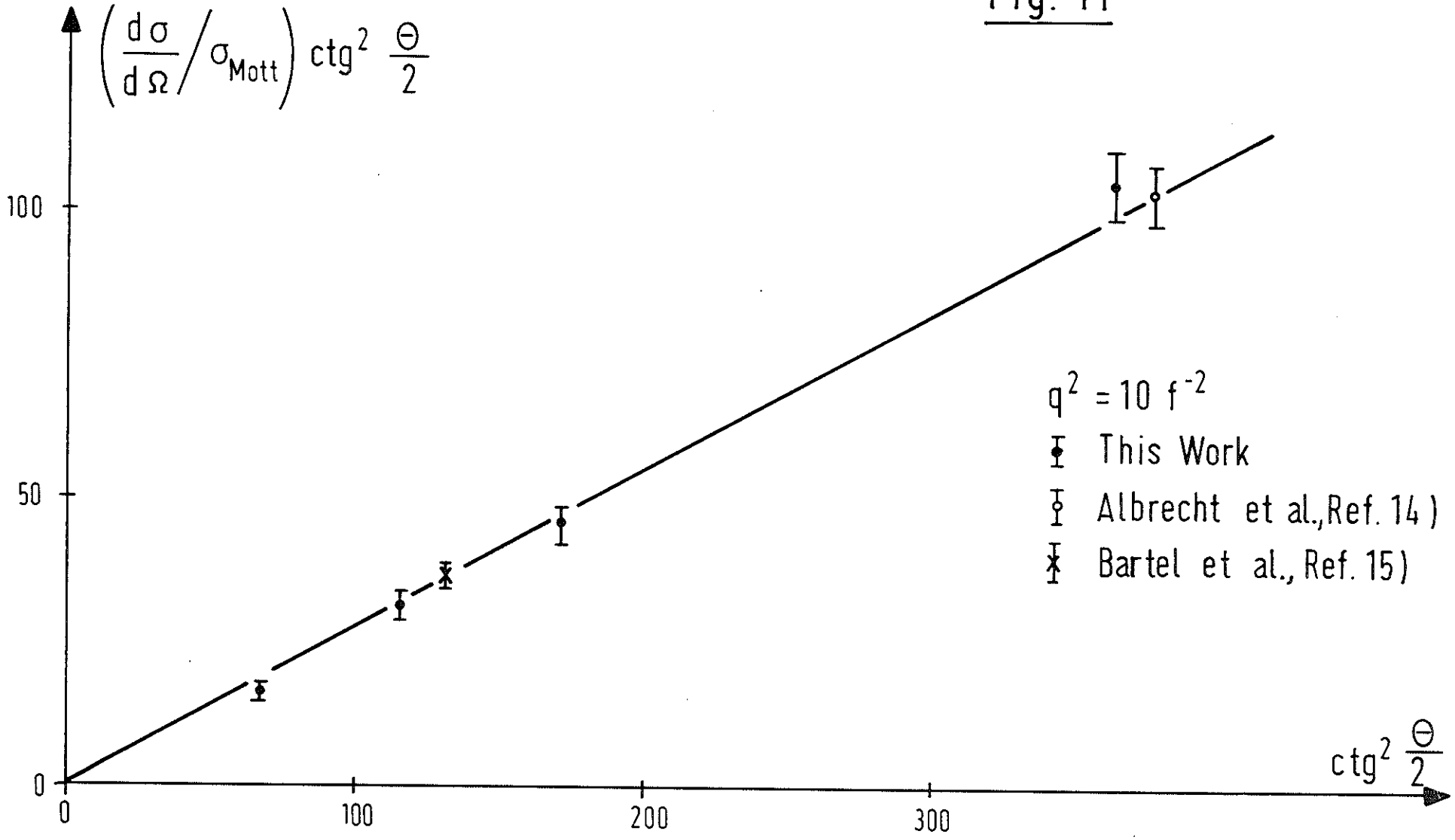
$\left(\frac{d\sigma}{d\Omega}/\sigma_{Mott}\right) ctg^2 \frac{\Theta}{2}$
100
50
0
0
100
200
300
$ctg^2 \frac{\Theta}{2}$
$q^2 = 10\ f^{-2}$
This Work
Albrecht et al., Ref. 14)
Bartel et al., Ref. 15)

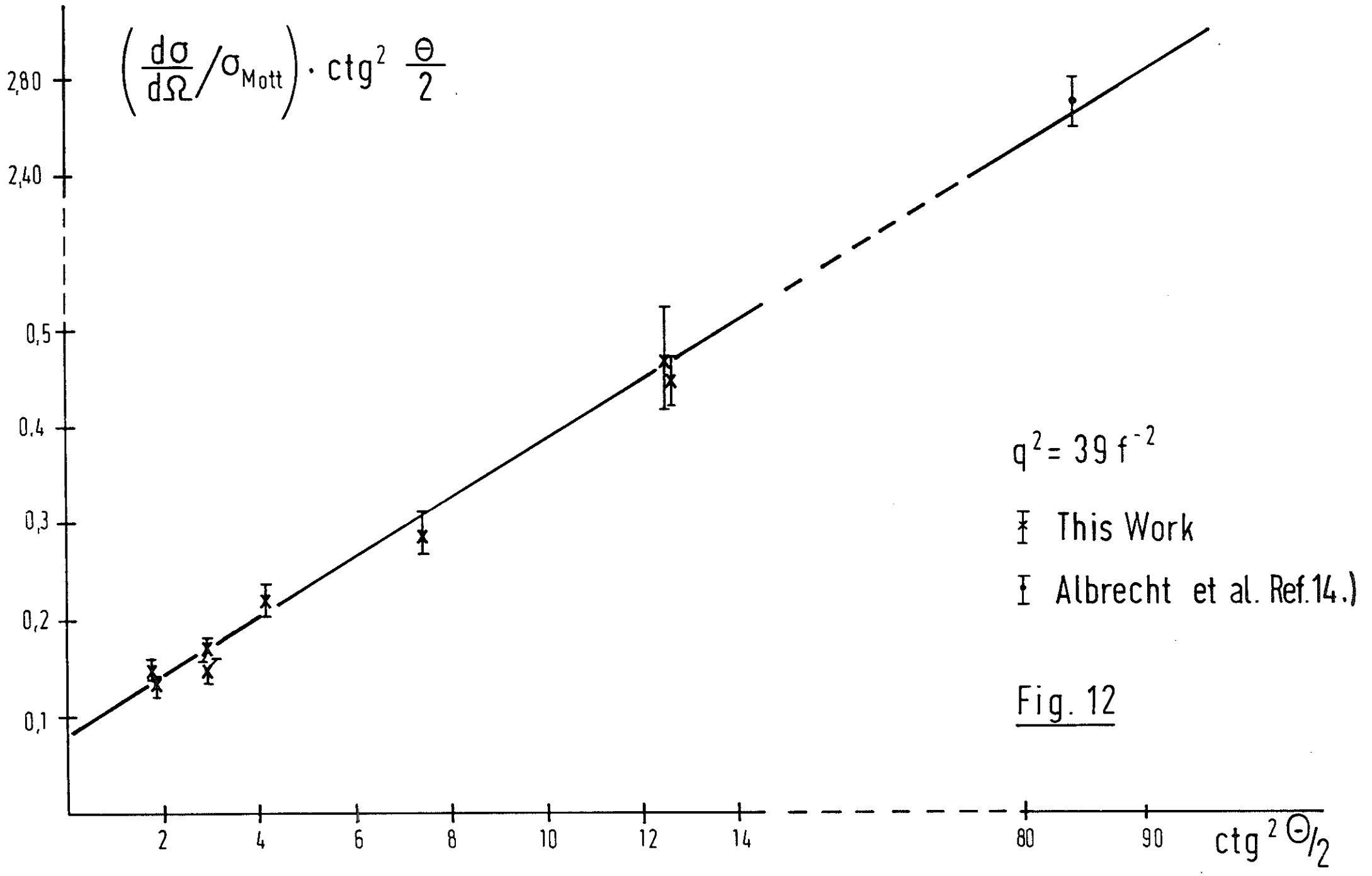
$\left(\frac{d\sigma}{d\Omega}/\sigma_{Mott}\right) \cdot ctg^2 \frac{\Theta}{2}$
2,80
2,40
0,5
0,4
0,3
0,2
0,1
2
4
6
8
10
12
14
80
90
$ctg^2 \Theta/2$
$q^2 = 39\ f^{-2}$
This Work
Albrecht et al. Ref.14.)

Fig. 12

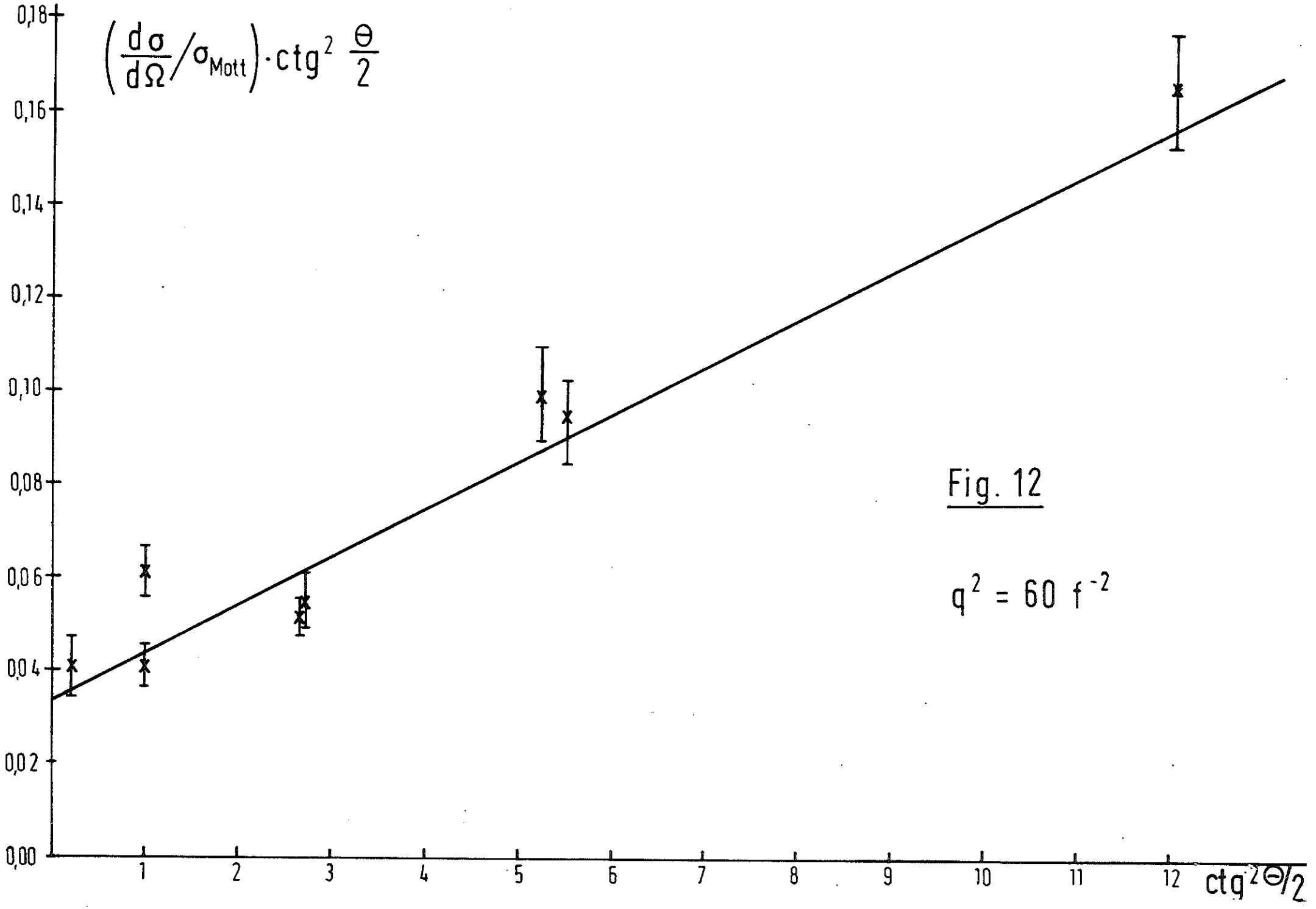

Fig. 12

$q^2 = 60\ f^{-2}$

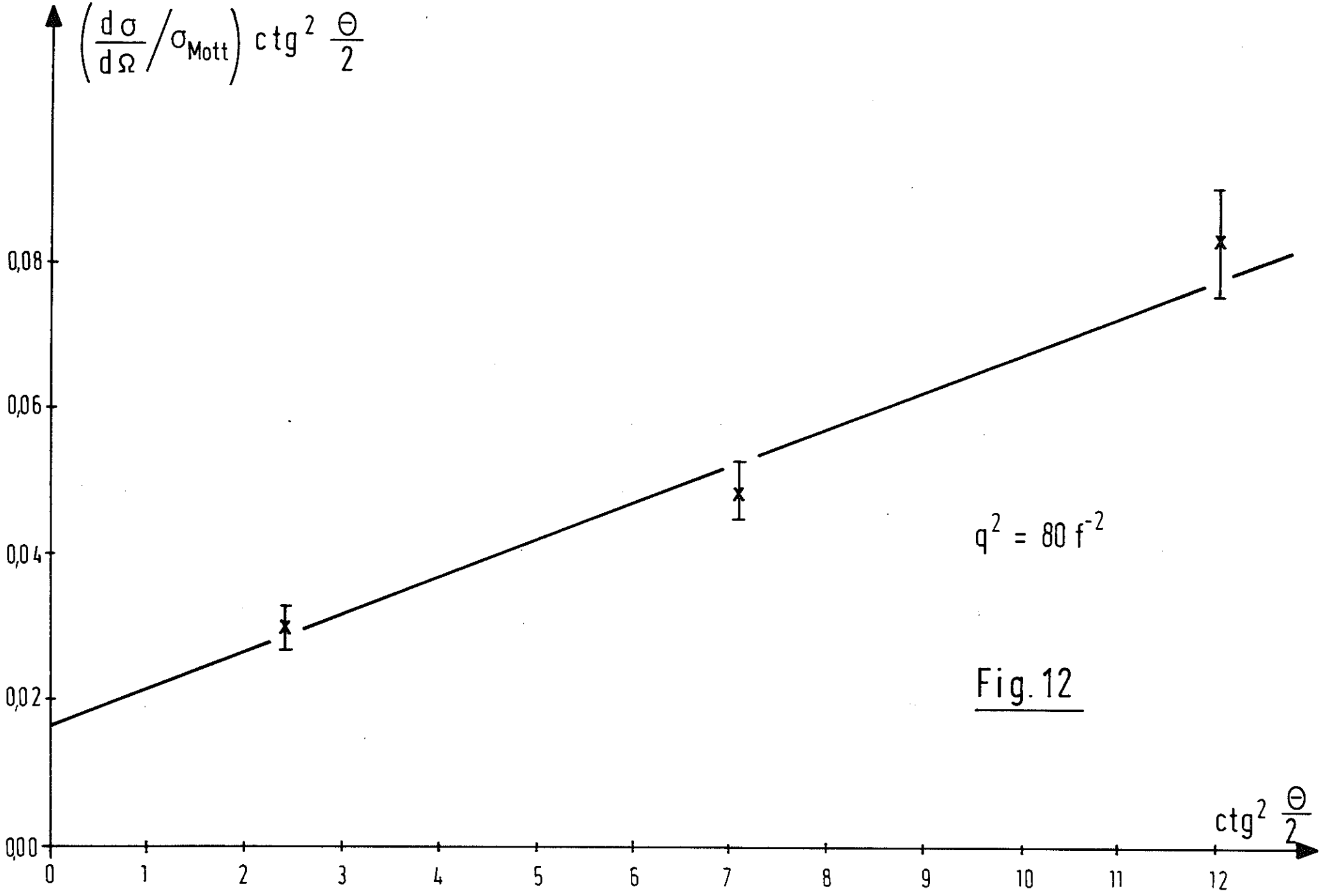
$\left(\frac{d\sigma}{d\Omega}/\sigma_{Mott}\right) ctg^2 \frac{\Theta}{2}$
0,08
0,06
0,04
0,02
0,00
0
1
2
3
4
5
6
7
8
9
10
11
12
$ctg^2 \frac{\Theta}{2}$
$q^2 = 80\ f^{-2}$

Fig. 12

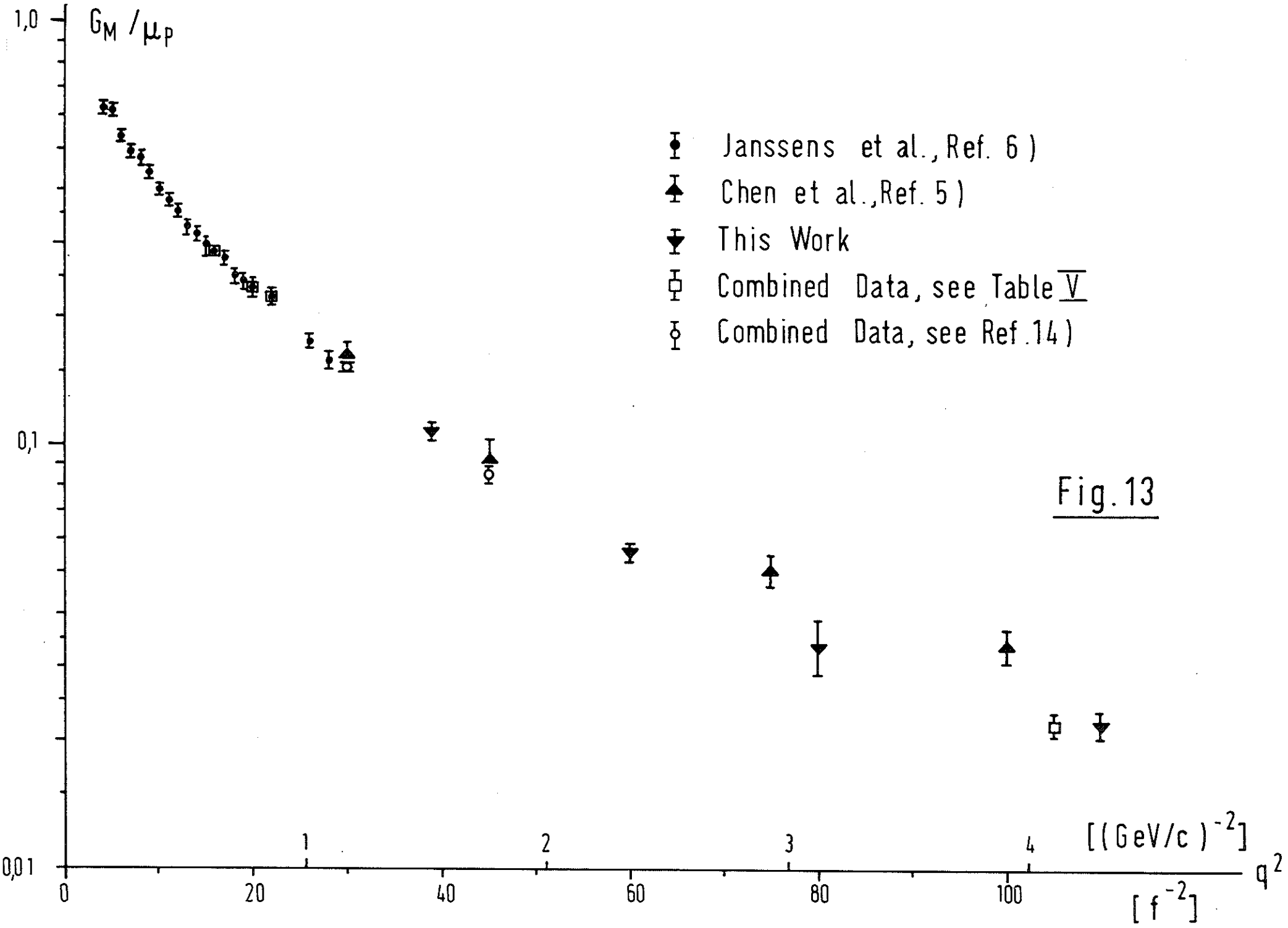
1,0
G_M / μ_P
0,1
0,01
Janssens et al., Ref. 6)
Chen et al., Ref. 5)
This Work
Combined Data, see Table V
Combined Data, see Ref. 14)
1
2
3
4
[(GeV/c)$^{-2}$]
q^2
0
20
40
60
80
100
[f^{-2}]

Fig. 13

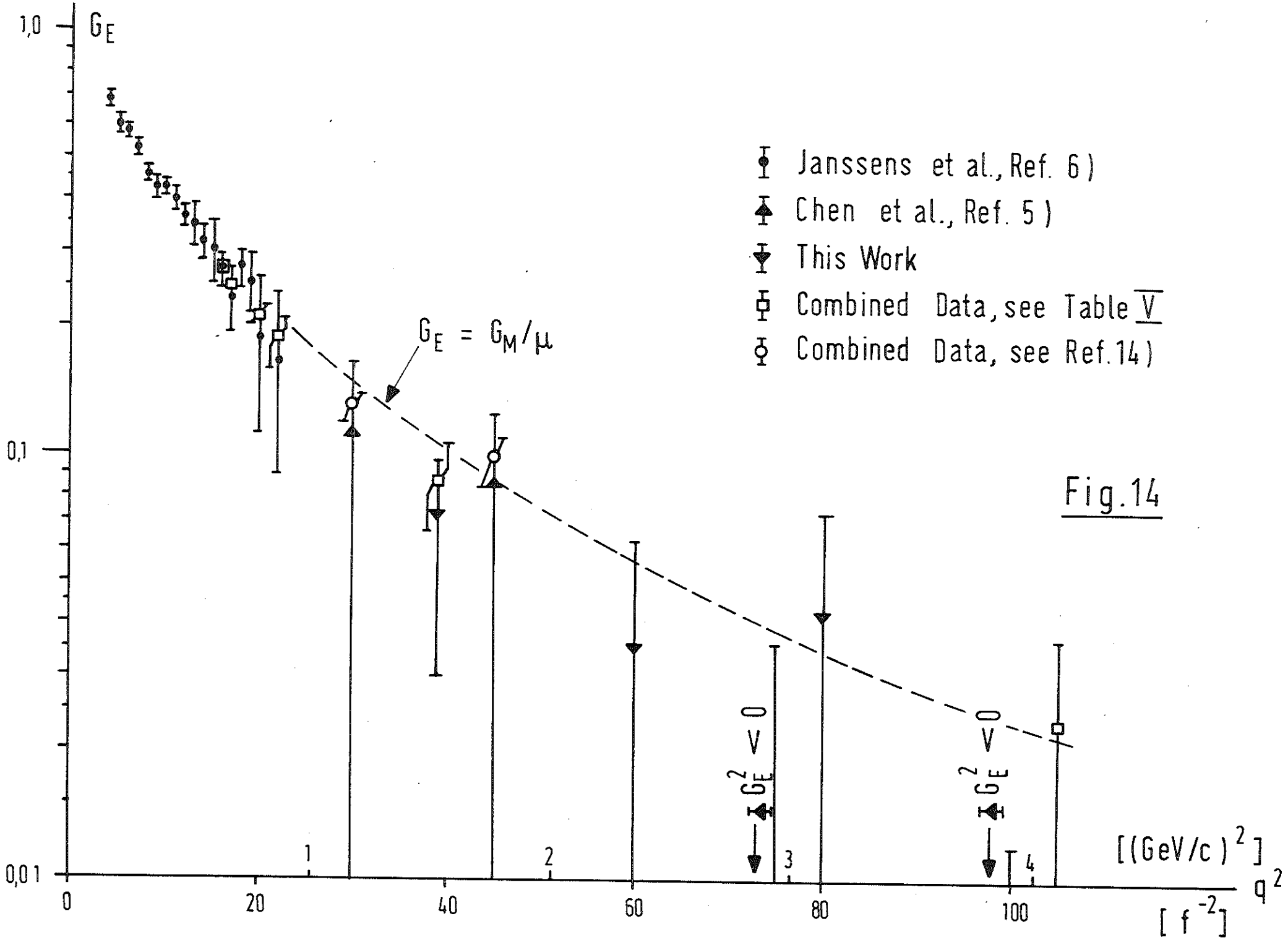
1,0
G_E
0,1
0,01
$G_E = G_M/\mu$
Janssens et al., Ref. 6)
Chen et al., Ref. 5)
This Work
Combined Data, see Table V
Combined Data, see Ref. 14)
$G_E^2 \approx 0$
$G_E^2 \approx 0$
0
20
40
60
80
100
1
2
3
4
q^2
$[(GeV/c)^2]$
$[f^{-2}]$

Fig. 14